

# Topical Review of Quantum Materials and Heterostructures Studied by Polarized Neutron Reflectometry

Grace L. Causer,\* Laura Guasco, Oliver Paull, and David Cortie

A review of the applications of polarized neutron reflectometry (PNR) for the investigation of quantum materials is provided. Recent studies of superconductors, strongly correlated oxides, hydrogen-induced modifications, topological insulators and chiral magnets are highlighted. The PNR technique uses a quantum beam of spin-polarized neutrons to measure the nanomagnetic structure of thin films and heterostructures, with a sensitivity to magnetization at the scale of  $10\text{--}2000\text{ emu cm}^{-3}$  and a vertical spatial resolution of  $1\text{--}500\text{ nm}$ . From simple beginnings studying the magnetic flux penetration at superconducting surfaces, today the PNR technique is widely used for investigating many different types of thin film structures, surfaces, interfaces, and 2D materials. PNR measurements can reveal a number of details about magnetic, electronic, and superconducting properties, in tandem with chemical information including the stoichiometry of light elements such as oxygen and hydrogen.

Quantum materials are solids where non-universal quantum effects give rise to novel functionalities that offer prospects for new forms of electronics, computation, simulation, and sensing. While, in fact, all chemical compounds exhibit quantum effects such as chemical bonding, the term quantum materials is best used to describe a special class exhibiting rare phenomena such as unconventional superconductivity, exotic magnetism, quantum critical points, and topological phase transitions.<sup>[1]</sup> These unusual materials share the common feature that they exhibit nonuniversal emergent quantum effects, beyond those found in normal solids, which offer potential uses in quantum technologies. It is widely anticipated that quantum technologies, utilizing these materials, will eventually be

## 1. Introduction

The growing demand for new quantum technologies, together with the quest for a fundamental understanding of solid matter, has given birth to a new field: the study of quantum materials.


translated into wide-ranging societal impacts by revolutionizing cybersecurity, drug discovery, materials modeling, and logistics.<sup>[2]</sup> Indeed, in the last 5 years, a new generation of quantum devices has begun to demonstrate some promising real-world implementations;<sup>[3]</sup> however, significant improvements in the underlying material science are still required to fully realize their potential.

---

G. L. Causer  
Physik-Department  
Technical University of Munich  
James-Franck-Straße 1, D-85748 Garching, Germany  
E-mail: grace.causer@tum.de

L. Guasco  
Max-Planck-Institut für Festkörperforschung  
Heisenbergstraße 1, D-70569 Stuttgart, Germany  
L. Guasco  
Max Planck Society Outstation at the Heinz Maier-Leibnitz Zentrum (MLZ)  
D-85748 Garching, Germany

O. Paull, D. Cortie  
Australian Centre for Neutron Scattering  
Australian Nuclear Science and Technology Organisation  
Lucas Heights, New South Wales 2234, Australia

 The ORCID identification number(s) for the author(s) of this article can be found under <https://doi.org/10.1002/pssr.202200421>.

© 2022 The Authors. physica status solidi (RRL) Rapid Research Letters published by Wiley-VCH GmbH. This is an open access article under the terms of the Creative Commons Attribution License, which permits use, distribution and reproduction in any medium, provided the original work is properly cited.

A common route to incorporate quantum materials into practical devices is to prepare thin films or heterostructures using established deposition techniques, such as magnetron sputtering, chemical vapor deposition, or molecular beam epitaxy. These deposition techniques allow for the controlled growth of layered materials and heterostructure components with atomically perfect interfaces. As nanoelectronics is rapidly approaching the 2D limit, the functionality of a heterostructure is often governed by its interfaces. In addition, several emergent phenomena such as 2D electron gases, magnetism, and superconductivity have been shown to exist only at certain interfaces.<sup>[4]</sup> As the Nobel Prize laureate Herbert Kroemer famously once stated, “the interface is the device,” and with the rise of quantum material heterostructures, this statement is now more true than ever.

Studying the complex nature of quantum materials demands a complementary range of investigative tools and techniques, with a sensitivity to surfaces and interfaces, to probe the chemical and electronic structure. Such techniques include (scanning) transmission electron microscopy (STEM), low-energy electron diffraction (LEED), angle-resolved photoemission spectroscopy (ARPES), scanning tunneling microscopy (STM), polarized neutron reflectometry (PNR), resonant elastic X-ray scattering (REXS), resonant X-ray reflectometry (XRR), extended X-ray absorption

DOI: 10.1002/pssr.202200421

fine structure (EXAFS), nitrogen-vacancy diamond microscopy, low-energy muon spectroscopy, and  $\beta$ -nuclear magnetic resonance ( $\beta$ -NMR), just to name a few. Among these techniques, the method of PNR offers some unique capabilities to characterize and study quantum materials in a range of external environments, i.e., pressure, temperature, atmosphere, and magnetic field.

PNR is a quantum beam technique which capitalizes on the coherent interference effects of spin-polarized neutron matter waves reflected from surfaces and interfaces. Analogous to optical reflection, the neutrons employed in PNR sense the effective refractive index of the reflecting medium, and undergo constructive and destructive interference from multiple interfaces in stratified media. From the frame of reference of the neutron, the refractive index of any magnetic material consists of both chemical (nuclear) and magnetic contributions. Using the experiment setup schematically illustrated in **Figure 1**, state-of-the-art PNR instrumentation therefore provides quantitative and sensitive information about the local magnetization and magnetic induction field at surfaces and interfaces, as well as across nanoscale film thicknesses. Additional low-temperature and/or high-pressure and magnetic field environments are routinely employed by PNR to investigate material behaviors under extreme conditions. Combining standard specular measurements, with grazing incidence and off-specular techniques, PNR can examine both vertical and periodic lateral junction arrays with spatial resolutions from 1 to 500 nm (vertical) and 10 nm to 1000  $\mu$ m (lateral). This positions PNR as a powerful tool for the study of nanomagnetism and spin-based effects which are characteristic features of many quantum materials.

This topical review is designed to introduce researchers with an interest in quantum materials to the PNR technique. As the field of quantum materials is expanding rapidly, this review is not intended to be comprehensive. There are already several past reviews that independently discuss the applications of PNR to quantum materials such as superconductors,<sup>[5]</sup> strongly correlated oxides,<sup>[6]</sup> complex magnets,<sup>[7,8]</sup> hydrogen capture,<sup>[9]</sup> and topological materials<sup>[10,11]</sup> and the interested reader is encouraged to refer to the latter reviews. However, the intention here is to provide a comparative overview of the applications of PNR to these distinct forms of quantum materials for the first time, providing the cross-linking to highlight the possibilities of examining complex heterostructures combining multiple types of quantum materials. The outline of the review is as follows. Section 2 provides a brief introduction to the principles of PNR. In Section 3, we highlight some recent applications of PNR toward the study of superconducting materials, strongly correlated oxides, hydrogen-induced modifications, topological insulators (TIs), and chiral magnets. The review concludes with Section 4 which discusses the future perspectives of PNR for the study of quantum materials.

## 2. Theoretical Principles of Polarized Neutron Reflectometry

The reflection of neutrons from polished surfaces was first observed by Enrico Fermi and Walter Zinn during the

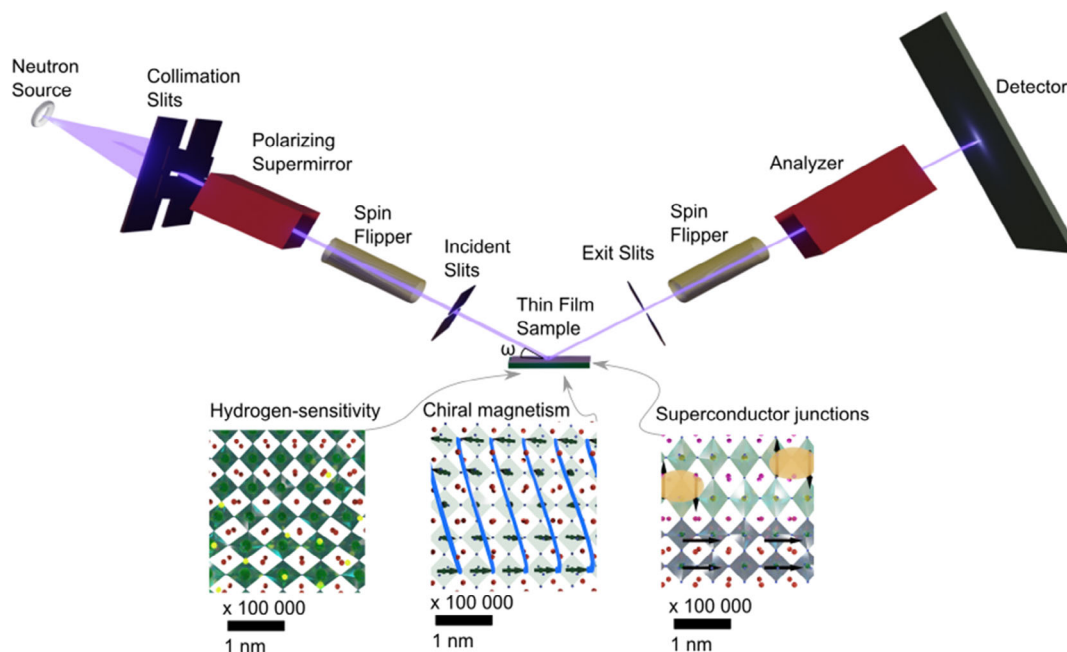


**Figure 1.** Schematic of the PNR setup. Divergent neutrons from the source pass through collimation slits creating a thin beam. The beam passes through a polarizing supermirror which transmits only one neutron spin-state, i.e., spin up (+) or spin down (–). An additional spin flipper can be used to select the alternate neutron spin-state when desired. The spin-polarized beam is reflected from the thin film or heterostructure sample, and the outgoing spin-state of the beam is analyzed using the spin-flipper and analyzing supermirror before the intensity is measured on a detector. The measurement is performed at a range of angles ( $\omega$ ) and/or neutron wavelengths to construct a full reflectivity pattern of the sample under investigation. Numerous quantum interface phenomena including hydrogen-induced modifications, chiral magnetism, and superconducting proximity effects can be studied using PNR.

Manhattan Project,<sup>[12]</sup> and was subsequently used to ascertain the scattering lengths and coherent scattering cross sections of several elements.<sup>[13]</sup> In the decade which followed, the concept was further expanded to include the reflection of neutrons from magnetic materials,<sup>[14]</sup> which laid the theoretical foundations for the use of neutron reflectometry, and in particular PNR, as experimental techniques for the study of magnetic and nonmagnetic surfaces. Early neutron reflectometry experiments by Hayter et al. in 1976 explored the ability of magnetic surfaces to spin-polarize beams of neutrons.<sup>[15]</sup> During the decade which followed, neutron reflectometry and PNR were developed as analytical techniques for studying interfacial phenomena in a variety of materials.<sup>[16–19]</sup>

PNR is the measurement of a reflected beam of neutrons which have been collimated and spin-polarized prior to interacting with a sample. PNR can be conducted with a single wavelength (monochromatic) or a white (polychromatic) beam of neutrons. The theory of PNR can be derived by quantum mechanical or optical means, and has been treated in detail in several previous works,<sup>[20–24]</sup> and as such only the main results will be summarized here. Furthermore, detailed historical accounts of the evolution of the PNR technique can also be found in previous works.<sup>[25,26]</sup> Here, we will consider a simple quantum mechanical treatment using the 1D Schrödinger equation representing the change in wave function along the  $z$ -axis perpendicular to the reflection interface which lies in the  $(x,y)$ -plane, such that

$$\left[ -\frac{\hbar^2}{2m_n} + V(z) \right] \Psi(z) = E\Psi(z) \quad (1)$$

A neutron interacting with a magnetic surface with magnetic induction  $\mathbf{B} = \mu_0(\mathbf{H} + \mathbf{M})$  will experience a potential given by

$$V = \frac{2\pi\hbar^2}{m_n} \rho_{\text{nuc}} \pm \boldsymbol{\mu}_n \cdot \mathbf{B} \quad (2)$$

where  $m_n$  is the neutron mass,  $\rho_{\text{nuc}}$  is the nuclear scattering length density (SLD), and  $\boldsymbol{\mu}_n$  is the neutron magnetic moment. It can be seen from Equation (2) that the potential incorporates a nuclear and magnetic term. This implies that when a neutron interacts with a stratified magnetic medium, the reflectivity will depend on the direction of net magnetization of the layer with respect to the spin-state of the neutron.

In general, the reflection of neutrons from a heterostructure comprised of  $m$ -layers can be expressed as a sum of plane waves given by

$$\Psi_0(z) = A_m e^{ik_{z,m}z} + B_m e^{-ik_{z,m}z} \quad (3)$$

where  $A_m$  and  $B_m$  are the coefficients for reflection and transmission, respectively, from the  $m$ th interface of the heterostructure. At grazing incidences of reflection, neutrons see an averaged density of the scattering lengths in a crystal lattice, called the nuclear SLD defined as

$$\rho_{\text{nuc}} = \sum_i N_i b_{n,i} \quad (4)$$

where  $N_i$  is the number density of the  $i$ th atom with coherent

neutron scattering length  $b_{n,i}$ . For a magnetic medium, an additional term is added to Equation (4) to account for the magnetic interaction between the neutron spin-state and the magnetism of the material, resulting in a magnetic SLD given by

$$\rho_{\text{mag}} = \frac{m_n}{2\pi\hbar^2} \sum_i N_i \mu_i = C \sum_i N_i \mu_i \quad (5)$$

where  $C = 2.645 \text{ fm } \mu_B^{-1}$  and  $N_i$  is the number density of atoms with magnetic moment  $\mu_i$ . These two SLDs combine to give a total nuclear and magnetic SLD of

$$\rho = \rho_{\text{nuc}} + \rho_{\text{mag}} = \sum_i N_i (b_i \mp C\mu_i) \quad (6)$$

where the  $\mp$  sign arises from the incident neutrons being spin-polarized parallel (+) and antiparallel (−) to the sample magnetization. For materials with a ferromagnetic (FM) or polarized paramagnetic component, the difference in SLD between the parallel ( $R^{++}$ ) and antiparallel ( $R^{--}$ ) alignment of the neutron spin-states with respect to the sample magnetization results in a difference in reflectivity for each spin channel. This difference is known as the spin asymmetry (SA) ratio which is expressed as

$$\text{SA} = \frac{R^{++} - R^{--}}{R^{++} + R^{--}} \quad (7)$$

Under certain circumstances, the sample magnetization may not lie strictly either parallel or antiparallel to the neutron spin-state, but rather at some arbitrary angle. In such scenarios, the component of the sample magnetization that is perpendicular to the neutron polarization axis will apply a torque to the neutron, causing it to flip upon interaction with the sample. This produces a so-called spin-flip reflected signal, commonly represented by  $R^{+-}$  and  $R^{-+}$ . Note that by convention, the state of the incoming neutron polarization is encoded in the first superscript ( $X$ ) in  $R^{XY}$ , whereas the state of the outgoing polarization is encoded in the second superscript ( $Y$ ) of  $R^{XY}$ , so that  $R^{+-}$  refers to a spin-flip process with a spin-up incident neutron (+) and a spin-down outgoing neutron (−). To observe such a process, a spin analyzer is necessary to measure the outgoing beam from the sample. In the case that no spin analysis is performed, it is customary to drop the second superscript and simply write  $R^X$ .

## 2.1. Specular Reflectometry

For specular reflectometry, as depicted in **Figure 2a**, the angle ( $\omega$ ) of the incident neutron wavevector  $\mathbf{k}_i$  is exactly half the reflected angle ( $2\theta$ , i.e.,  $\omega = \theta$ ) of the final neutron wavevector  $\mathbf{k}_f$ . The modulus of the resulting wavevector transfer  $Q$  is normal to the sample surface, such that  $Q = Q_z$ , which is expressed as

$$Q_z = |\mathbf{k}_f - \mathbf{k}_i| = \frac{4\pi}{\lambda} \sin \omega \quad (8)$$

This scattering geometry is sensitive to structural and magnetic periodicities perpendicular to the plane of the film (i.e., along the  $z$ -axis). As such, it only detects the average density and magnetism in the plane of the film, which requires lateral

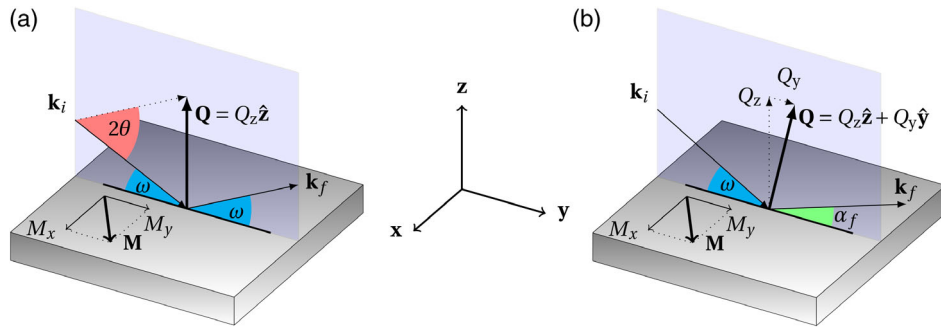


**Figure 2.** PNR scattering geometries. a) Specular PNR geometry, where the angle ( $\omega$ ) of the incident neutron wavevector  $\mathbf{k}_i$  is exactly half the reflected angle ( $2\theta$ , i.e.,  $\omega = \theta$ ) of the final neutron wavevector  $\mathbf{k}_f$ , resulting in a momentum transfer normal to the sample surface with modulus  $Q_z$ . b) Off-specular PNR geometry, where the angle ( $\omega$ ) of the incident neutron wavevector  $\mathbf{k}_i$  is not exactly half the reflected angle ( $2\theta$ , i.e.,  $\omega \neq \theta$ ) of the final neutron wavevector  $\mathbf{k}_f$ , resulting in a small additional  $y$ -component of momentum transfer  $Q_y$ , forming in the plane of the film parallel to the neutron beam.

homogeneity in order to accurately analyze and fit reflectivity patterns.

The Born approximation for specular reflection from a multilayer slab geometry with total thickness  $L$  can be expressed as<sup>[20,27]</sup>

$$|R|^2 = \left| \frac{4\pi}{Q_z} \int_0^L \rho(z) e^{iQ_z z} dz \right|^2 \quad (9)$$

The Born approximation is useful because of its simplicity; however, it is only a first approximation, and typically deviates from the exact solution at low  $Q$ , where dynamic scattering effects are important. To this end, most modern software programs implement more complicated exact matrix methods (for brevity, not discussed here, refer to ref. [20]). There are several different software packages that can be utilized to fit neutron reflectivity data.<sup>[28–31]</sup> These packages all utilize an exact numerical formalism to calculate the reflectivity but vary in their statistical rigor and programmatic implementation of the tools used to fit experimental data.

## 2.2. Off-Specular Reflectometry

For off-specular reflectometry, as depicted in Figure 2b, the angle ( $\omega$ ) of the incident neutron wavevector  $\mathbf{k}_i$  is no longer exactly half the reflected angle ( $2\theta$ , i.e.,  $\omega \neq \theta$ ) of the final neutron wavevector  $\mathbf{k}_f$ . This results in an additional  $y$ -component of the momentum transfer ( $Q_y$ ) that is sensitive to structural and magnetic periodicities in the plane of the film parallel to the neutron beam. In the off-specular geometry, the expressions for the modulus of the  $y$ - and  $z$ -components of the momentum transfer are

$$Q_y = \frac{2\pi}{\lambda} (\cos \alpha_f - \cos \omega) \quad (10)$$

$$Q_z = \frac{2\pi}{\lambda} (\sin \alpha_f + \sin \omega) \quad (11)$$

where, if  $\alpha_i = \alpha_f = \omega$ , the beam is specularly reflected and Equation (11) reduces to Equation (8) while Equation (10) goes to zero.

The distinct components of in-plane and out-of-plane momentum transfer (i.e.,  $Q_y$  and  $Q_z$ ), which are accessible with off-specular PNR, allow sensitivity to depth as well as lateral periodicities with nuclear and/or magnetic SLD contrast parallel to the neutron beam. Due to relaxed beam collimation along the  $x$ -axis, resolution in  $Q_x$  is generally not observed in PNR, while resolution in  $Q_y$  is limited by the neutron coherence length, which is typically on the micrometer length scale.<sup>[9]</sup> It is, however, possible to use the grazing incidence diffraction geometry to resolve much smaller (nm-scale) features in  $Q_x$ ; however, the geometry is quite different from a standard reflectometry experiment. For a discussion of grazing incidence geometry, refer to ref. [9].

## 3. Applications of PNR for the Study of Quantum Materials

### 3.1. Superconductors

Superconductors are prototypical examples of quantum materials due to their ability to conduct dissipationless current originating from nonuniversal quantum mechanical interactions (e.g., the formation of Cooper pairs). Historically, the PNR technique had its birthplace in the study of superconductors.<sup>[19,32]</sup> The very first published PNR pattern by Felcher et al. in 1984 investigated the Meissner effect in a Nb superconductor.<sup>[32]</sup> This was a hallmark moment as it showcased the utility of the PNR technique for probing nanoscale magnetic phenomena, which provided the impetus to apply the technique more widely to other quantum materials, such as magnets and oxides, which will be discussed in the later sections of this review.

The reflectometry pattern published by Felcher et al. showed that, above the critical temperature  $T_C$ , the neutron reflectometry pattern of a Nb film was independent of the neutron spin-state.<sup>[32]</sup> Meanwhile, below  $T_C$ , the reflection pattern differed for spin-up and spin-down neutrons, owing to the scattering contrast introduced by the variable induction field at the superconducting surface. This finding has since been widely reproduced by various groups. For example, **Figure 3a** illustrates PNR data reported by Zhang et al. above the  $T_C$  of a Nb thin film showing it



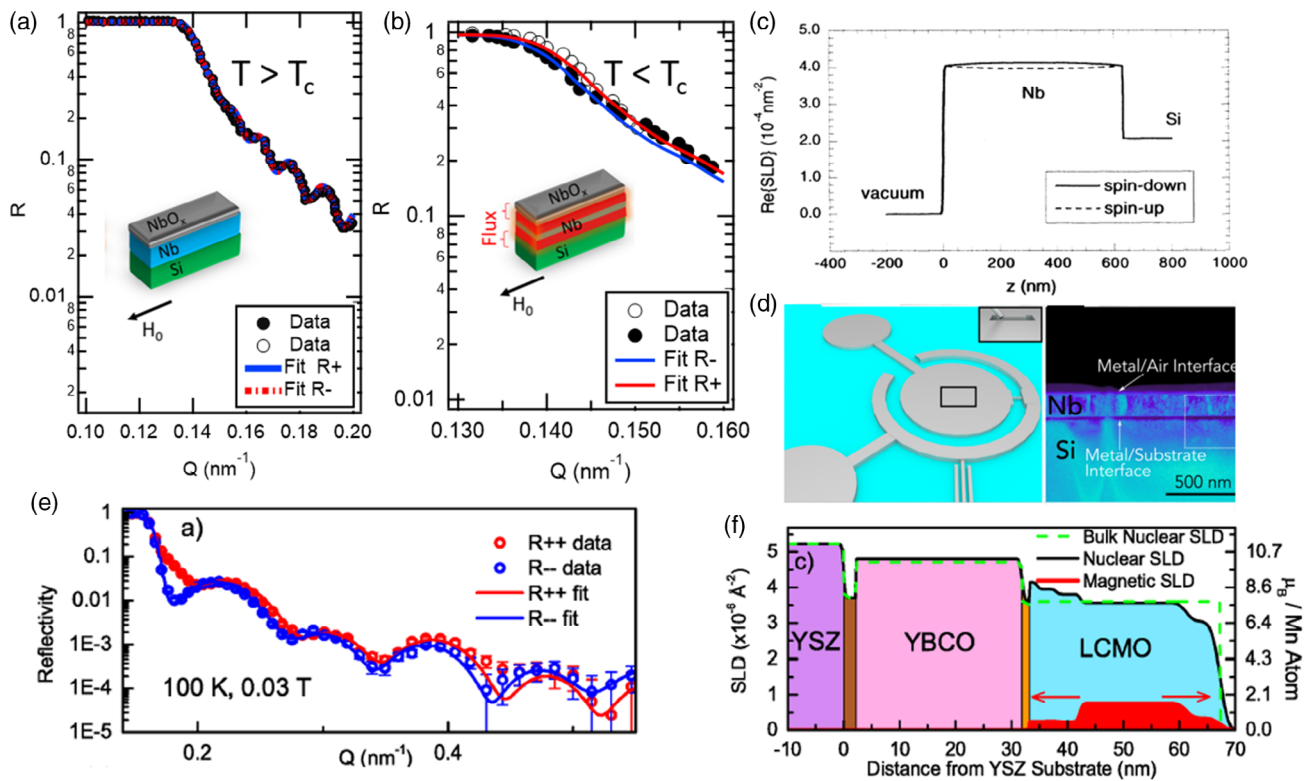


**Figure 3.** a) PNR pattern for a Nb thin film on Si above  $T_c$ . b) Below  $T_c$  the PNR signal shows a clear splitting in the neutron spin-states which can be fitted to determine the nuclear and magnetic SLD profiles. c) Neutron SLD profile for a Nb thin film in the superconducting state. The spin-down and spin-up profiles refer to the  $R^-$  and  $R^+$  reflectivities, respectively. Adapted with permission.<sup>[33]</sup> Copyright 1995, American Physical Society. d) An illustration of the modern application of Nb superconductors in the transmon qubit geometry, where the black box illustrates the components comprised of Nb and  $NbO_x$  layers, similar to those depicted by the cross-sectional TEM image on the right. Adapted with permission.<sup>[34]</sup> Copyright 2022, American Chemical Society. e) An example of PNR measured in a high-temperature superconductor/ferromagnet YBCO/STO/LCMO heterostructure. f) Bulk nuclear SLD (dashed green), nuclear SLD (black), and magnetic SLD (red fill) of the PNR pattern in (e). Reproduced with permission.<sup>[50]</sup> Copyright 2018, Royal Society of Chemistry.

can be fitted such that  $R^+ = R^-$ .<sup>[33]</sup> In contrast, below  $T_c$ , the neutron spin-states become unequal, showing a clear splitting in Figure 3b. This can be fitted to a model to extract the neutron SLD (refractive index), as shown in Figure 3c. This general approach allows one to extract the magnetic penetration depth  $\lambda_m$ . Felcher et al. first reported  $\lambda_m$  to be  $410 \pm 40 \text{ \AA}$  which was later confirmed by Zhang et al.<sup>[33]</sup> A complicating factor in some PNR analyses is the presence of a  $NbO_x$  surface layer, which can introduce a nonmagnetic interface region commonly referred to as a “dead layer” which has been detected in several PNR studies (see the references in ref. [33]).

An exciting development since 2019 has been the rise in popularity of quantum computing using “simple” elemental superconductors such as Nb and Al. In particular, Nb/ $NbO_x$  and Al/ $AlO_x$  are widely used in the transmon qubit architecture,<sup>[34]</sup> as depicted in Figure 3d. These architectures were the basis of the first claims (by the Google team in 2019) of a 54-qubit system that was presented as the first example of “quantum supremacy,” i.e., the ability to do a specific type of calculation faster than a classical computer.<sup>[3]</sup> It is expected that superconductor/insulator/superconductor Josephson junctions will remain a key operational component in superconducting

quantum computing based on the transmon architecture. It appears that this has started to reinvigorate PNR as a tool to study these types of junctions used in nanoelectronics. The first experiments on similar structures have recently been published on Al/ $Al_2O_3$ /Ni/Ga junctions.<sup>[35]</sup> Currently, there is an international effort to identify and solve the material factors inhibiting qubit performance, such as high error rates, high noise, and low coherence times,<sup>[36]</sup> and PNR is expected to help provide insights into these important problems.

Along with ongoing studies into “classical” superconductors, the discovery and rise of high-temperature oxide superconductors such as  $YBa_2Cu_3O_{7-\delta}$  (YBCO) in the 1990s motivated new types of PNR experiments, in particular, searching for proximity effects between different classes of quantum materials. One system that has been extensively investigated is the superconductor/ferromagnet YBCO/ $La_{1-x}Sr_xMnO_3$  (LSMO) heterostructure,<sup>[37–40]</sup> with a view to studying the competing order parameters of superconductivity with ferromagnetism.

A key early result in this field was the detection of a magnetic interface effect in YBCO/LSMO superlattices grown on  $SrTiO_3$  (STO), where the PNR patterns showed a modification at the interfaces.<sup>[37]</sup> In the preliminary studies, it was unclear whether

this involved suppression of the LSMO moment, or an enhanced moment in the YBCO layer.<sup>[37]</sup> At this point, a large focus switched to clarifying the nature of the FM proximity effect. Several high-profile studies detected modifications to the magnetic domain structure and spin-density of the LSMO layer.<sup>[38–40]</sup> A major point of discussion was the subsequent measurement of a moment induced on Cu atoms near the YBCO interface<sup>[41,42]</sup> which was taken as an indication of orbital reconstruction, and later detected by XMCD and PNR.<sup>[43]</sup>

One important realization in this field was that STO substrates pose a major problem for reflectometry studies, as they are subject to twinning and surface-faceting below the tetragonal-cubic phase transition at  $\approx 100$  K, which leads to a broadening of the neutron beam and other secondary effects. For this reason, later studies increasingly began to use alternate substrates including (La,Sr)(Al,Ta)O<sub>3</sub> (LSAT). The work by Uribe-Laverde et al. first used LSAT substrates to avoid the problems associated with STO, and compared closely with the earlier studies.<sup>[44]</sup> They concluded that the only model that could describe the PNR data was a magnetic depletion layer at the LSMO interface. More recent work by Prada et al. has also shown that the deposition sequence of YBCO/LSMO layers impacts on the formation of the depletion layers,<sup>[45]</sup> and other groups have shown that the delicate chemistry of the LSMO plays an important role.<sup>[46]</sup> The question of whether there is an induced moment in the superconducting interface warrants additional investigation. While some PNR studies did not directly detect any induced moment on the YBCO side, it is pointed out that the magnetic contrast is small, making this difficult to detect, and indeed, the data is compatible with a much smaller induced moment in the Cu, as proposed by Liu et al.<sup>[41,42]</sup>

We note that an induced moment in the superconducting layer can also potentially arise from the paramagnetic Meissner effect, or so-called “inverse proximity” effect. It is a challenging topic within PNR to detect such effects, given their small associated magnetization. The feasibility of detecting the inverse proximity effect has been explored in detail in other superconductor/ferromagnet bilayers.<sup>[47]</sup> One approach that has been shown to enhance the sensitivity of PNR to small induced moments is the resonant waveguide enhancement method.<sup>[48]</sup> Here, multilayer stacks are deliberately designed such that their resultant SLD profiles create neutron standing waves, enabling multiple reflections, in a region of interest. This leads to an enhancement of the neutron wave function in the resonant layer, and in turn to an enhanced sensitivity to that layer. This technique potentially allows considerably more certainty when detecting small variations in the superconducting component; however, to the best of our knowledge, this approach has not yet been applied to YBCO/LSMO heterostructures.

Another recent development has been studying superconducting proximity effects in response to the presence of nonmagnetic insulator spacer layers in superconductor/insulator/ferromagnet junctions. Initial work by Prajapat et al. showed a large modulation of the FM magnetization below the critical temperature of the superconductor in LSMO/STO/YBCO trilayers.<sup>[49]</sup> Subsequent work on La<sub>1-x</sub>Ca<sub>x</sub>MnO<sub>3</sub> (LCMO)/STO/YBCO confirmed this effect,<sup>[50]</sup> revealing a depleted interfacial FM magnetization as highlighted in Figure 3e,f. Here, the application of an external magnetic field above the superconducting critical field

was shown to remagnetize the FM interface. This shows that superconducting order is implicated in the magnetically depressed interface regions in the FM layer. In a similar vein, recently, it was also shown that disorder introduced into the superconductor via targeted ion beam irradiation could also be used to restore the depleted FM moment of the interfacial region.<sup>[51]</sup>

The most recent development in the study of superconductors has been the discovery of interfacial and 2D superconductors. Recently, a PNR study elucidated the origin of the unusual superconductivity of Ni/Bi interfaces,<sup>[52]</sup> showing that interfacial alloying can lead to a new superconducting phase of Ni<sub>3</sub>Bi. Currently, there is also growing interest in achieving superconductor/ferromagnet bilayers for spin-triplet superconductivity.<sup>[35]</sup> The prospects for future PNR studies to reveal novel insights into superconducting heterostructures remain strong in the coming decade.

### 3.2. Strongly Correlated Transition Metal Oxide Interfaces

The strong electron-electron interactions in transition metal oxides (TMOs) lead to a variety of emergent quantum phenomena including superconductivity, colossal magnetoresistance, multiferroicity, and metal–insulator transitions.<sup>[53]</sup> The ability to precisely engineer heterostructures of epitaxial TMOs has led to these materials being heavily researched as a material science platform. Here, PNR has proven to be particularly effective for the study of layered TMOs. At the interface between TMOs, the delicate balance between structural, orbital, charge, and spin degrees of freedom can be altered by small external perturbations such as chemical doping, strain, and electromagnetic fields. This gives rise to a whole “zoo” of quantum phenomena which are not observed in bulk<sup>[54]</sup> and are highly interesting for electronics and spintronics applications.<sup>[55–57]</sup> Many TMOs share the perovskite structure, which entails that the different components of oxide heterostructures have very similar electronic densities. For this reason, the study of TMO heterostructures with laboratory X-ray sources is hindered by the limited scattering contrast. This difficulty is overcome with either resonant scattering synchrotron measurements, or with the use of neutron scattering techniques, such as PNR.<sup>[58,59]</sup>

Aside from high- $T_C$  superconducting interfaces, spin valves, and proximity effects, which were discussed in the previous section, we have identified three main relevant branches of research where PNR has been a key technique in understanding oxide interfaces: interface magnetism, exchange spring and bias, and interlayer exchange coupling (IEC).

In many oxide systems, one can observe the emergence of unexpected magnetic phases at the interface of two nonferromagnets due to charge transfer effects, which can enable super exchange or double exchange interactions. Due to the depth-dependent sensitivity to magnetism, even down to 1 unit cell,<sup>[60,61]</sup> it is easily understood why PNR is one of the go-to choices to study these heterostructures. A special mention goes to the AMO/BMO (with  $A = \text{Sr}$ ,  $B = \text{La}$ ,  $\text{Nd}$ ,  $M = \text{Mn}$ ) systems, often referred to as delta-doped layers, which have been extensively investigated by PNR. In these systems, by varying the thickness of the AMO and BMO components—both

antiferromagnetic (AFM) insulators—it is possible to tune both the metallicity and the magnetic correlations.<sup>[62]</sup> The general trend in these superlattices is that if their components are thin enough, the charge transfer across interfaces makes it possible to tune all the magnetic phases observed in the complex manganite phase diagram.<sup>[63]</sup> One recent example is the case of SrMnO<sub>3</sub>/NdMnO<sub>3</sub> (SMO/NMO) superlattices,<sup>[64]</sup> as shown in Figure 4a,b, where PNR was used to attribute the emergent magnetism to the SMO component, due to the tuning of double exchange interactions across the AFM interfaces. Notable are the cases of metallic ferromagnets attained in these digitally synthesized superlattices,<sup>[62,64]</sup> with ordering temperatures higher than those of the corresponding solid solutions A<sub>1-x</sub>B<sub>x</sub>MnO<sub>3</sub>, thanks to the reduced structural disorder.<sup>[65]</sup> On top of tuning double exchange mediated ferromagnetism, May et al. found an unexpected asymmetric magnetic depth profile, corresponding to unequal structural roughness at the upper and lower interfaces.<sup>[66]</sup> In the work by Santos et al., where PNR was used in combination with polarized neutron diffraction, the authors were able to show the possibility to modulate canted A-type antiferromagnetism with depth-dependent canting angle.<sup>[67]</sup>

Further important works reported the discovery of emergent ferromagnetism at CaRuO<sub>3</sub>/CaMnO<sub>3</sub> (CMO)<sup>[60]</sup> and LaNiO<sub>3</sub>/CMO<sup>[61]</sup> interfaces. In both cases, attentive PNR fitting of the magnetic depth profile showed FM correlations at both interfaces between the paramagnet and the antiferromagnet, with thickness corresponding to one monolayer. This emergent magnetism results from the reduced valence state of Mn atoms, due to the small electron leakage from the nearby metallic layer.

Spin and orbital reconstruction also play an important role at the interface between FM and non-FM TMO layers. The

interfacial reconstruction, which affects the valence electronic structure, can lead to a degradation of magnetic properties, and in extreme cases to the formation of magnetic “dead layers”.<sup>[37]</sup> PNR studies have shown, for example, reduced interface magnetic moments, which can be used to engineer desirable functionalities, such as exchange bias.<sup>[68,69]</sup> Figure 4c shows the final result of the PNR data fitting for a LCMO/CMO bilayer deposited on STO. Depending on the stacking order of the FM and non-FM layers in the heterostructure, it is possible to tune the interface spin reconstruction, which, in both cases, results in a depressed magnetic interfacial region. Spin frustration was found to be 95% larger in the case of the heterostructure with a STO/CMO/LCMO stacking sequence,<sup>[68]</sup> as compared to the STO/LCMO/CMO stacking sequence shown in Figure 4d. The enhanced spin frustration in the STO/CMO/LCMO heterostructure arose due to compressive strain within the crystalline lattice of the FM LCMO layer, which resulted in an enhanced exchange bias to the AFM CMO surface layer.

In contrast, ferromagnetism can extend beyond its nominal depth, as observed in ferroelectric/FM TMO interfaces and manganite/ruthenate films,<sup>[70]</sup> which are of particular importance for spintronics devices.<sup>[71–73]</sup> PNR was also used to visualize the complex magnetic structure of so-called exchange springs, obtained in different systems with a fine tailoring of the electronic reconstruction at the interface between two FM TMOs with different magnetocrystalline anisotropies.<sup>[74,75]</sup> These measurements allowed, through careful fitting procedures and comparisons of several model structures, the mapping of the layer-by-layer magnetization depth profile, which was shown to gradually change from an in-plane to an out-of-plane alignment of moments.

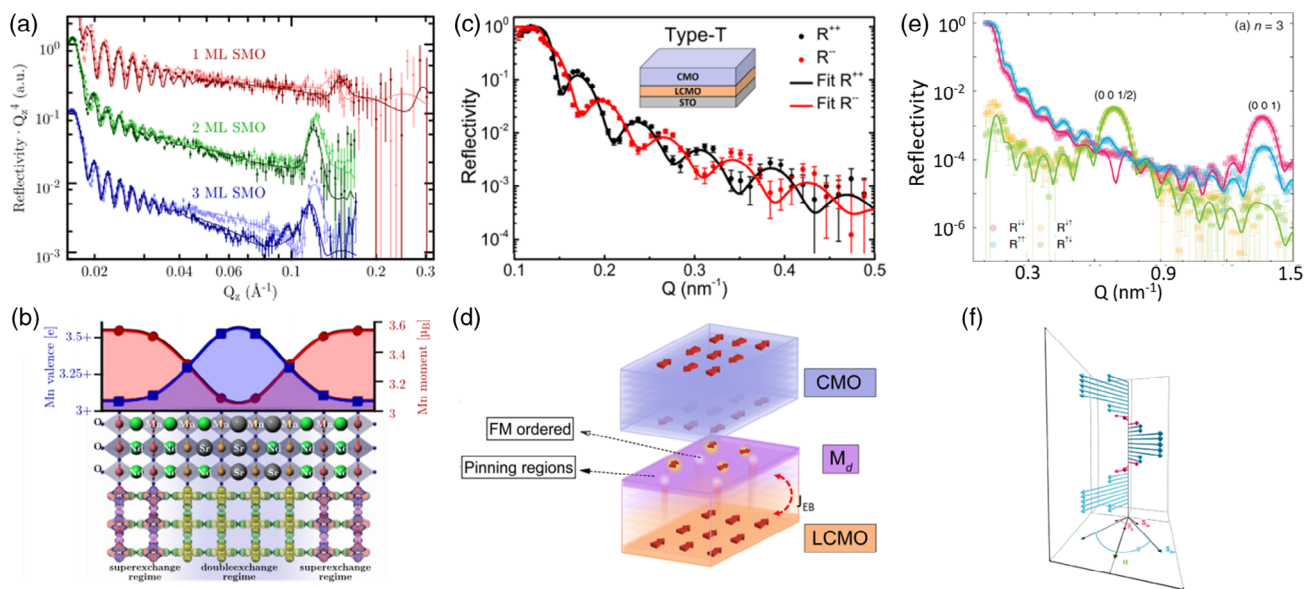


**Figure 4.** Key role of PNR in TMO heterostructure studies. a) PNR measurement of SrMnO<sub>3</sub>/NdMnO<sub>3</sub> superlattices unveiled emergent interface ferromagnetism in SrMnO<sub>3</sub>, as schematized in b). Reproduced with permission.<sup>[64]</sup> Copyright 2016, American Physical Society. c) R<sup>++</sup> and R<sup>--</sup> channels and model fit of the interface between a FM La<sub>0.7</sub>Ca<sub>0.3</sub>MnO<sub>3</sub> (LCMO) layer and an AFM CaMnO<sub>3</sub> (CMO) layer. d) The corresponding model of interfacial spin frustration and reconstruction responsible for the sizable exchange bias observed in the LCMO/CMO system under tensile strain. Adapted with permission.<sup>[68]</sup> Copyright 2021, American Physical Society. e) PNR of a superlattice composed of LaNiO<sub>3</sub> (3 ML)/La<sub>0.66</sub>Sr<sub>0.33</sub>MnO<sub>3</sub> (9 ML). f) Proposed micromagnetic model showing noncollinear doubling of magnetic structure. Adapted with permission.<sup>[76]</sup> Copyright 2016, American Physical Society.

Recent advancements in oxide deposition technology have led to the successful engineering of long-range coupling in superlattices made of these more complex materials. This type of coupling is not only interesting to understand the physics of magnetic interactions over long distances, but it is also particularly useful in the realization of the so-called synthetic antiferromagnets. Synthetic antiferromagnets are central to AFM spintronics because they merge the tunability of ferromagnetism and the stability of antiferromagnetism to realize “the best of both worlds.” Even though the IEC leaves signatures in the magnetometry measurement, these are often not straightforward or unequivocal. A direct proof of IEC is, however, easily obtained by PNR, with the appearance of additional magnetic Bragg peaks corresponding to higher order periodicities than the structural order. Figure 4e,f shows a representative example of a clear doubling of the magnetic structure that generally manifests in the appearance of superlattice Bragg peaks with fractional indices. Figure 4e shows the noncollinear IEC between manganite layers observed in  $\text{LaNiO}_3/\text{La}_{0.66}\text{Sr}_{0.33}\text{MnO}_3$  heterojunctions, due to strong exchange interactions with the nickelate spiral magnetic order.<sup>[76]</sup> The visualization of the proposed magnetic structure is presented in Figure 4f, where the blue arrows represent LSMO magnetic moments, and the pink arrow represents the spiral magnetic order in the spacer.

As a second example, Chen et al. demonstrated through the use of PNR the realization of a synthetic antiferromagnet obtained by stacking FM  $\text{La}_{0.66}\text{Ca}_{0.33}\text{MnO}_3$  and insulating  $\text{CaRu}_{0.5}\text{Ti}_{0.5}\text{O}_3$ .<sup>[77]</sup> Here, a full AFM alignment of consecutive FM layers was obtained due to spin-polarized tunneling through the spacer. A further IEC heterojunction was recently reported in  $\text{SrRuO}_3/\text{STO}$  systems,<sup>[78]</sup> albeit with slightly less clear PNR results. Another very recent PNR study reported the magnetic fan structure observed in LSMO homojunctions with depth-dependent Sr and hole doping.<sup>[79]</sup> Here, the PNR not only confirmed the doubling of magnetic periodicity, but also gave a hint about the origin of the IEC itself. In fact, the detailed depth profiles obtained from PNR fitting showed a net magnetic moment at the highest doping depth, nominally AFM, suggesting a canting which was later confirmed by neutron diffraction. This canting, which is strongly hole-doping dependent, as already observed by Santos et al.,<sup>[67]</sup> is then imprinted onto the FM part of the homojunction to form the so-called magnetic fan. To this end, we particularly want to highlight the advantage of measuring PNR data with polarization analysis, which allows all four reflectivity channels (i.e.,  $R^{++}$ ,  $R^{+-}$ ,  $R^{-+}$ , and  $R^{--}$ ) to be obtained. Only with the help of polarization analysis were the data displayed in Figure 4e able to unveil the noncollinear nature of the magnetic doubling represented in Figure 4f. This is in comparison to earlier works performed without polarization analysis, such as in Figure 4a,c, where this important information was lost in the unanalyzed  $R^+$  and  $R^-$  reflectivities.

### 3.3. Hydrogen-Induced Modifications at Interfaces

Hydrogen, the lightest element, is a quantum defect in many materials, capable of undergoing tunneling, and introducing drastic modifications as an electrically active dopant. For this

reason, hydrogen intercalation is a versatile control parameter for the physical properties of thin films and materials in general. The impact on the host is multifold, depending on the nature of the hydrogen species involved, which can be neutral atomic  $\text{H}^0$ , or positively charged  $\text{H}^+$  (proton), but also depends on the position that H occupies (e.g., interstitial, grain boundaries, voids, and defects). Several recent discoveries have sparked great interest in this additional degree of freedom, for example, for the controlled modification of magnetic anisotropy or exchange coupling,<sup>[80–87]</sup> of electrical resistivity,<sup>[88–90]</sup> or even of transition temperature in unconventional superconductors.<sup>[91–93]</sup>

Neutron methods are particularly well suited to the study of hydrogen capture or hydrogen-induced modifications, due to the negative scattering length of hydrogen, and the possibility to obtain contrast enhancement through isotopic substitution with deuterium. In particular, PNR can consistently retrieve information about hydrogen-induced changes in the nuclear and magnetic profiles of thin films. For a more detailed review on PNR capabilities extended to light elements, we address the reader to ref. [9].

An early application of PNR was to study hydrogen-controlled giant-magnetoresistive effects in  $\text{Fe}/\text{Nb}$ <sup>[82,94]</sup> and  $\text{Fe}/\text{V}$ .<sup>[81]</sup> Here, the hydrogen is absorbed in the spacer layer, increasing its thickness and hence directly varying the RKKY coupling between FM layers. In this case, the advantage of using PNR was twofold: on one hand it allowed for the quantification of swelling in the spacer layer, while at the same time providing clear information about the interlayer magnetic order.

Another clear advantage of PNR for the study of hydrogen-induced modifications is the possibility to perform in situ and in operando studies. Other direct techniques with comparable (or better) sensitivity, in the case of X-ray photoelectron spectroscopy (XPS) or nuclear methods such as elastic recoil detection analysis (ERDA), allow the detection of small concentrations of absorbed hydrogen (e.g.,  $\leq 0.1$  at%), however require high vacuum conditions. In this respect, one interesting case study was the hydrogen exposure of LSMO thin films, which entails a reversible metal–insulator transition. Initial XPS studies, performed ex situ, showed a discrete amount of absorbed hydrogen in the manganite lattice,<sup>[95]</sup> indicating an electron-doping induced metal–insulator transition. However, shortly after this, Mazza et al. demonstrated with the use of in situ neutron reflectometry that the effect of hydrogen exposure is in fact oxygen depletion in a  $\text{D}_2$  gas atmosphere.<sup>[96]</sup> The possibility to perform in situ studies is central in cases such as this one, where the formation of metastable phases can lead to substantially different conclusions.

In addition to these advantages, PNR provides information about the magnetic properties of interfaces, which is fundamental for understanding the working principle of many proton-based solid-state devices. In this respect, key examples are those concerning the hydrogen-induced switching of perpendicular magnetic anisotropy.<sup>[87,97]</sup> In particular, in operando studies performed by Causer et al. showed the origin of reduced perpendicular magnetic anisotropy at the  $\text{Co}/\text{Pd}$  interface. Through an accurate fitting of the PNR curves obtained in  $\text{N}_2$  (Figure 5a, green curve) and 3.5%  $\text{H}_2/\text{N}_2$  atmospheres (Figure 5a, blue curve), the authors found an enhanced in-plane magnetic



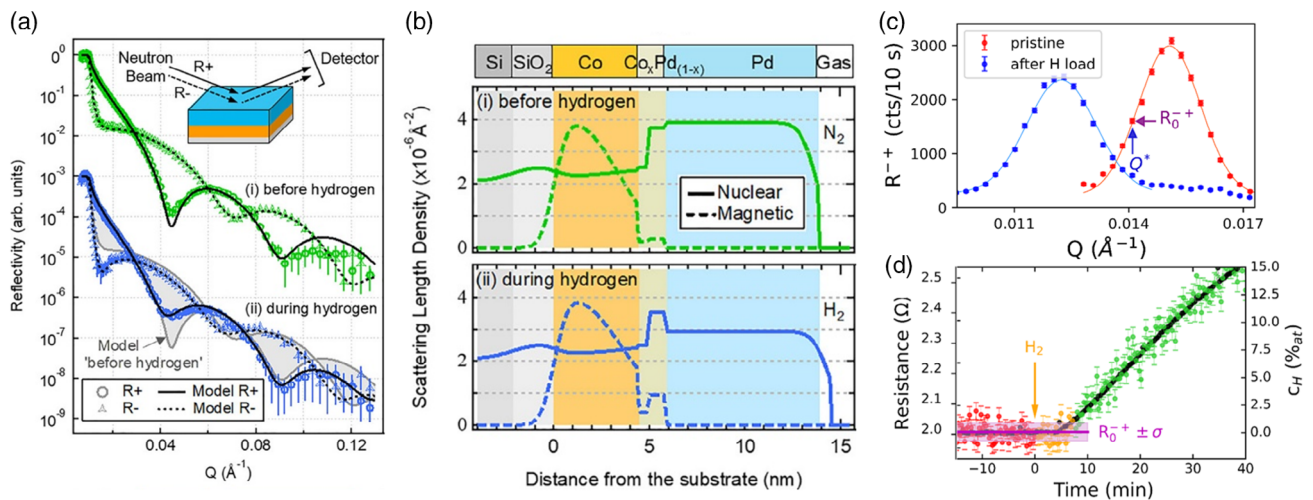


**Figure 5.** Capabilities of PNR in detecting hydrogen capture and its effect in thin films. a) PNR of Co/Pd bilayers before (i) and during (ii) hydrogen exposure. b) Nuclear (solid) and magnetic (dashed) SLD depth profiles obtained from the PNR data presented in (a). Reproduced with permission.<sup>[87]</sup> Copyright 2019, American Chemical Society. c) Resonant reflectometry showing the shift of the waveguide maximum  $Q_{\text{res}}$  before (red) and after (blue) hydrogen exposure of Nb films. d) Fixed- $Q$  scan at  $Q^*$  (i.e., arbitrary point defined in (c) near the resonance position) and in situ resistance measurement during hydrogen exposure. Reproduced under the terms of the CC-BY 4.0 License.<sup>[98]</sup> Copyright 2022, The Authors. Published by Springer Nature Limited.

moment upon hydrogen absorption in the thin alloyed interface at the boundary between the Co and Pd layers, as shown in Figure 5b. This indicates that the perpendicular magnetic anisotropy switching effect arises only at the interfacial region where the Co and Pd atoms are mixed, and not across the entire thickness of the Co layer.

There are two major limitations of PNR in this flourishing field. The first is the sensitivity limit: small amounts of hydrogen can be difficult to detect while still having significant electronic effects on the host material. The second limitation is the long counting times required for acquiring PNR data which limits the ability to study the fast kinetics of the absorption process. In this direction, there is some promising technique-development research aimed at increasing the sensitivity of PNR to hydrogen-induced modifications by using resonant waveguide enhancement methods.<sup>[98–100]</sup> Figure 5c shows the waveguide peak of a Nb resonator measured by means of PNR.<sup>[98]</sup> By adding a thin FM layer with noncollinear magnetization (obtained, for example, with an easy axis canted to the applied magnetic field), a resonant enhancement of  $R^{-+}$  spin-flip intensity is observed around the momentum transfer  $Q_{\text{res}}$ . As the position of  $Q_{\text{res}}$  depends on the scattering potential, when the scattering potential of the sample is modified through the absorption of hydrogen, one can observe a shift in the  $Q_{\text{res}}$  position, as shown in Figure 5c. The shift is, in the low concentration limit  $c_{\text{H}} < 30$  at%, directly proportional to the hydrogen content. By measuring the intensity variation at an arbitrary point  $Q^*$  on the resonance peak (Figure 5d), the hydrogen absorption kinetics can be retrieved. As the resonance is a sharp and intense feature, the shift of the resonance peak can be tracked with a significantly reduced counting time, typically a few seconds, and with quite high sensitivity, around 1 at%, as shown in Figure 5d. To demonstrate the precision of the resonant waveguide enhancement method and its ability to track changes of the sample properties, the authors of ref. [98] measured PNR simultaneously with the

widely used, albeit indirect, electrical resistivity sampling approach. As shown in Figure 5d, after the introduction of hydrogen, the resonance position displays a linear time dependence which tracks with the sample resistance (i.e., a property of the sample known to depend sensitively on the hydrogen content). While the two methods rely on completely different physics, their linear time dependencies can be used to track changes to the sample and cross-validate the amount of absorbed hydrogen.

These recent examples demonstrate that PNR is a useful tool to study proton-based device components, especially in synergy with other in situ techniques, such as FM resonance,<sup>[87]</sup> transport,<sup>[98]</sup> X-rays,<sup>[95]</sup> and more. The foreseen technical improvements to many reflectometers around the world will also allow more precise and less time-consuming measurements to be conducted in the future, opening the way to in operando studies.

### 3.4. Topological Insulators

The discovery of topological phases of matter was the basis of the 2016 Nobel Prize in Physics awarded to Thouless, Haldane, and Kosterlitz. One aspect of this discovery was the realization that the mathematical field of topology could be applied to characterize electronic structures and classify them using simple groups of integers known as topological invariants (e.g., Chern numbers). This led to the identification of several distinct topological phases, including 2D and 3D TIs, Weyl, nodal, and Dirac topological semimetals.<sup>[101]</sup> Importantly, the unique topological classifications are actually reflected in distinctive physical properties, including Dirac surface states, Fermi arc states, Weyl nodes, spin-angular momentum locking, helical spin polarization, magnetoelectric coupling, spin–torque coupling, and giant magnetoresistance. This has placed topological materials at the forefront of efforts to develop new forms of electronics for data storage, as well as classical and quantum computing.

The vast majority of existing PNR studies on topological materials have focused on a single class of material—the 3D strong TI—and its interaction with magnetism. TIs are bulk insulators at 0 K with a bulk band gap; however, they exhibit metallic Dirac surface states with a helical spin texture. Currently, the most heavily explored materials for 3D TIs are the chalcogenide semiconductors  $\text{Sb}_2\text{Te}_3$ ,  $\text{Bi}_2\text{Te}_3$ , and  $\text{Bi}_2\text{Se}_3$ . It was shown that magnetic doping, with elements such as Cr, Mn, or V, could induce long-range magnetic order and convert the TI into a quantum anomalous Hall insulator<sup>[102,103]</sup> or potentially to an axion insulator, depending on the relative magnetization direction at the top and bottom surfaces.<sup>[104]</sup> The former state has a quantized Hall conductance, whereas the latter has a vanishing Hall conductance, but exhibits an unusual magnetoelectric effect.<sup>[104]</sup> Later work has focused on utilizing the magnetic proximity effect between a TI/ferromagnet to control the magnetic functionality, such as the induced anomalous Hall effect and spin-transfer torque. For this reason, magnetic TIs have become the subject of a growing number of PNR studies. Two reviews are available that partially cover the application of PNR to these quantum materials,<sup>[10,11]</sup> however, as the field is rapidly evolving, below an updated summary is provided.

One of the earliest PNR studies of TIs was the work by Li et al. who investigated a magnetic insulator/TI heterostructure  $\text{EuS}/\text{Sb}_{2-x}\text{V}_x\text{Te}_3$ , where V doping was used to drive the TI  $\text{Sb}_2\text{Te}_3$  magnetic.<sup>[105]</sup> The authors observed a dramatic enhancement of the proximity exchange coupling strength, overcoming the limitation of magnetic insulator/nonmagnetic TI heterostructures, where the proximity effect is considered to be weak.<sup>[106]</sup> In addition, the proximity effect was accompanied by a decrease in the interfacial magnetism of EuS and to the emergence of an artificial AFM order.

Another early PNR study of TIs was the work by Collins-McIntyre et al. who investigated Cr-doped  $\text{Sb}_2\text{Te}_3$  layers, finding a uniform magnetic moment throughout the film layer.<sup>[107]</sup> This uniform magnetization is significant given the earlier theories that proposed that Dirac-surface electronics could substantially modify the surface magnetic state. While promising, one practical challenge with this magnetic system is its relatively low Curie temperature. For this reason, several groups have begun to investigate magnetic proximity effects by coupling a high-temperature magnet to a TI, and the latter group soon investigated  $\text{Co}/\text{Cr}-\text{Sb}_2\text{Te}_3$  structures, showing a moderate enhancement of the Curie temperature from 87 to 93 K.<sup>[108]</sup>

A key PNR result was the study of  $\text{EuS}/\text{Bi}_2\text{Se}_3$  FM/TI heterostructures that showed the interface of the TI could possess room-temperature magnetism induced by proximity to the magnetic insulator.<sup>[109]</sup> This was a promising development compared to traditional doping of the chalcogenides which generally leads to low Curie temperatures, below 100 K. Therefore, the proximity effect was taken as a potential route to achieve room temperature functionality. However, one of the main goals of introducing magnetism is to achieve the quantum anomalous Hall effect, and to-date transport studies on  $\text{EuS}/\text{Bi}_2\text{Se}_3$  have shown little or no anomalous Hall contribution.<sup>[110]</sup>

An outstanding challenge in this field of electronic materials is that the defects in the TI can lead to unwanted bulk conductivity, and certain effects such as the quantum anomalous Hall effect require a very precise level of controlled electron-hole doping.

For this reason, there is a focus on adjusting the material science of the TI by exploring solid solutions such as  $(\text{Bi}, \text{Sb})_2(\text{Se}, \text{Te})_3$ , together with magnetic dopants to precisely position the chemical potential (Fermi level) of the TI. This means that there is a challenge to find chemically compatible magnetic layers, which enable well-controlled doping and interface charge transfer. Key work in this area included studies employing CrSb on  $(\text{Sb}, \text{Bi})_2\text{Te}_3$  multilayers, which displayed a controllable exchange interaction.<sup>[111]</sup>

Aside from using traditional transitional metal elements as the source of magnetism, recent work has also begun to explore rare-earth components. In particular, a study on Dy-doped  $\text{Bi}_2\text{Te}_3$  revealed a complex magnetism, using a combination of muon spectroscopy and PNR.<sup>[112]</sup> At room temperature, the magnetism is disordered with slow magnetic fluctuations, which is more complicated than simple paramagnetism and superparamagnetism. PNR data at low temperatures showed clear SA, indicating a large magnetic moment on the Dy sites.<sup>[112]</sup> Subsequent work has also examined layers containing a mixture of transition metal and rare-earth dopants.<sup>[113]</sup>

An interesting development is the replacement of the ferromagnet with AFM components in TI heterostructures. Work on  $\text{CrSb}/\text{TI}$  structures showed that, even though the CrSb was AFM, it could magnetize the TI surfaces.<sup>[114]</sup> In related work, using PNR and other techniques, it was shown that a MnTe layer interfaced with  $(\text{Sb}, \text{Bi})_2\text{Te}_3$  led to a shift in the hysteresis loop and a shift in the transport properties—called a topological exchange bias effect.<sup>[115]</sup> More recent work has also examined the termination-dependent switching of  $\text{CrSe}/(\text{Sb}, \text{Bi})_2\text{Te}_3$  interfaces.<sup>[116]</sup> As the magnetism of proximity effects and antiferromagnetism are challenging to detect in PNR, new methods including machine learning have been applied to tackle this problem.<sup>[117]</sup> A further challenge in this area is the extremely low magnetization that arises in these dilute magnetic topological materials. **Figure 6a** shows the PNR data for a magnetic topological heterostructure recorded at  $T = 7.5$  K below the ordering temperature (i.e., 12 K) of the sample,<sup>[115]</sup> showing that the resulting spin-splitting is almost undetectable when plotted on a log scale. To highlight the differences, it is necessary to plot the SA as in **Figure 6b**. This small SA (5%) arises from magnetizations as low as  $10 \text{ emu cm}^{-3}$  corresponding to the SLD profile plotted in **Figure 6c**. Detecting this level of magnetization requires long counting times and near-perfect polarization (and associated corrections) in the experimental setup. Atomically flat interfaces, such as those shown in **Figure 6d**, are also advantageous for resolving these low levels of SAs.

Developing on the theme of replacing ferromagnets with AFM components, a most recent discovery in 2020 was that of an intrinsic AFM TI  $\text{MnBi}_2\text{Te}_4$ .<sup>[103]</sup> Bulk  $\text{MnBi}_2\text{Te}_4$  is perfectly compensated, while PNR measurements show a vanishingly small magnetization in 10 nm-thick films of  $\text{MnBi}_2\text{Te}_4$ .<sup>[118]</sup> It is expected that sufficiently thin films of  $\text{MnBi}_2\text{Te}_4$ , however, should lead to an uncompensated layer appearing that may be detectable with PNR. A major challenge, however, is the complex oxide layer that naturally forms at the ambient exposed interface.<sup>[118]</sup> Neutron reflectometry was used to characterize the thickness of this oxide, and importantly, the charge transfer associated with the oxide layer was shown to affect the anomalous Hall effect of the underlying TI structure.<sup>[118]</sup>

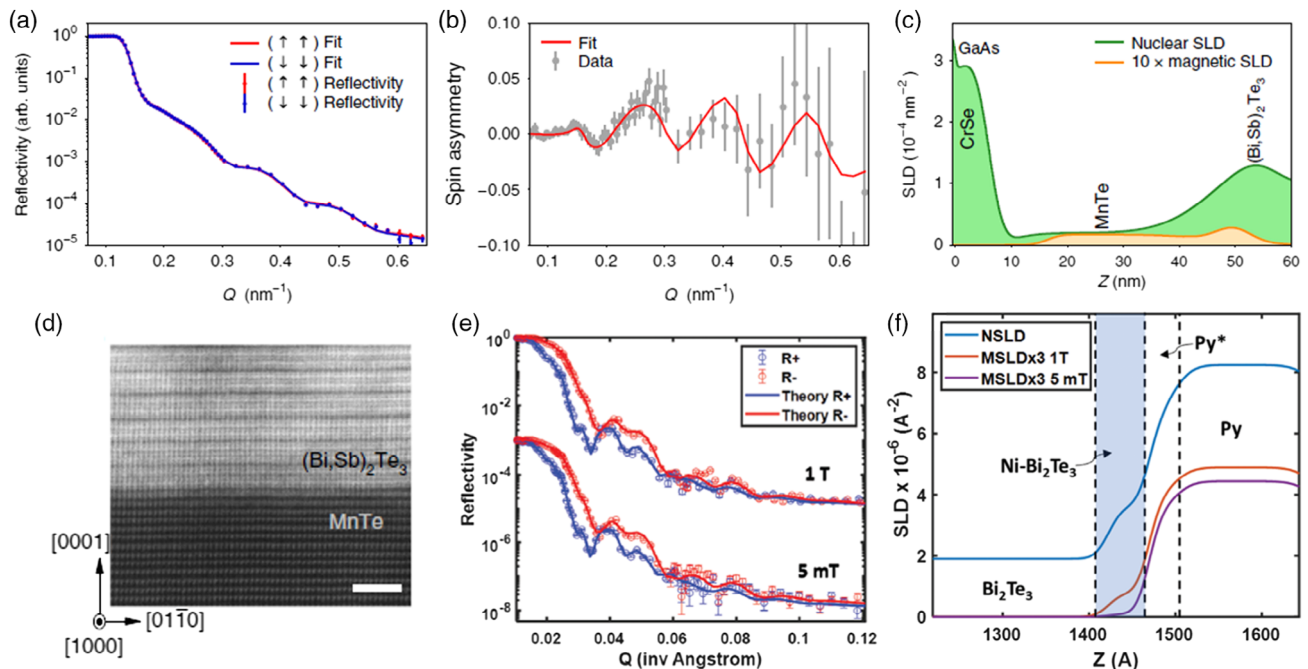


**Figure 6.** a) PNR of MnTe on a  $(\text{Sb, Bi})_2\text{Te}_3$  TI measured at 7.5 K in a 700 mT in-plane applied field, and b) corresponding SA profile. c) The corresponding nuclear and magnetic ( $\times 10$ ) SLD profile shows a magnetic contribution at the interface of the  $(\text{Sb, Bi})_2\text{Te}_3$  TI. The onset of the anomalous Hall effect was observed in the magnetic TI heterostructure below 12 K. It is noted that bulk MnTe is AFM with a Néel temperature  $T_N \approx 307$  K. d) Cross-sectional TEM image of the MnTe/ $(\text{Sb, Bi})_2\text{Te}_3$  heterostructure. Reproduced under the terms of the CC-BY 4.0 License.<sup>[115]</sup> Copyright 2018, The Authors. Published by Springer Nature Limited. e) Example of a PNR pattern from a NiFe/ $\text{Bi}_2\text{Te}_3$  heterostructure recorded at 7 K. f) SLD profile of the NiFe/ $\text{Bi}_2\text{Te}_3$  heterostructure recorded at 7 K shows a nonmagnetic region attributed to an AFM region at the interface. Reproduced with permission.<sup>[120]</sup> Copyright 2022, Wiley-VCH.

A practical drawback with some of the existing platforms of magnetic proximity effects in TIs is air sensitivity, or chemical incompatibility with existing industrial processes. For this reason, a new stream of research has emerged which studies heterostructures of TIs with common spintronic materials, already used industrially, with high Curie temperatures and well-understood oxidation behavior. The most popular strand is the interaction of the TI with a high-temperature garnet oxide film, such as yttrium iron garnet (YIG).<sup>[119]</sup> In parallel, some work has examined the interaction with standard CMOS-compatible metals such as Ni and Cu<sup>[120]</sup> grown on top of a chalcogenide such as  $\text{Bi}_2\text{Te}_3$ . Figure 6e shows the PNR pattern of a NiFe/ $\text{Bi}_2\text{Te}_3$  bilayer, where a strong spin splitting is evident. A major challenge is understanding the quantum chemistry and diffusion of the layers in such structures. The SLD profile in Figure 6f shows a nonmagnetic region at the interface which has been attributed to the formation of AFM Ni–Te bonds. PNR was used to show that the application of a magnetic field partly restores the magnetization in the interfacial region.<sup>[120]</sup>

While TIs offer strong possibilities for fundamental exploration, and perhaps future devices, clearly the material science of their interfaces still poses major challenges. Neutron reflectometry, with its innate depth sensitivity, is a promising way to characterize these interfaces in the future. There is still enormous scope to expand PNR studies on this topic, as only a small portion of the possible topological phases have been explored. For example, only recently, PNR was used for the first time to examine

heterostructures consisting of nonmagnetic topological crystal-line insulators such as SnTe, in proximity to magnetic TIs,<sup>[121]</sup> or simple ferromagnets.<sup>[122]</sup> Meanwhile, to the best of our knowledge, there are currently no PNR studies of other important classes of topological materials such as topological semimetals and topological superconductors, or their many combinational heterostructures.

### 3.5. Chiral Spin Systems

Relativistic spin–orbit interactions synonymous of chiral helimagnets enforce the antisymmetric Dzyaloshinskii–Moriya interaction leading to noncollinear magnetic order and a variety of quantum phenomena including, quantized winding numbers, emergent electrodynamics, and topological protection. Subsequently, chiral helimagnets, or more broadly speaking, chiral spin systems, are a further class of quantum materials where PNR has emerged as a pivotal technique to resolving their long-wavelength noncollinear magnetic order. A limited number of materials display chiral spin order including the family of cubic chiral magnets<sup>[123]</sup> such as MnSi, FeGe, MoGe,  $\text{Fe}_{1-x}\text{Co}_x\text{Si}$ ,  $\text{Cu}_2\text{OSeO}_3$ , EuPtSi, and  $\text{GaV}_4\text{S}_8$ ,<sup>[124]</sup> the monoaxial chiral magnets<sup>[125]</sup> such as  $\text{CrNb}_3\text{S}_6$  and  $\text{YbNi}_3\text{Al}_9$  as well as FM heavy-metal heterostructures.

In the bulk cubic and monoaxial magnets, chiral helimagnetic order appears as a ground state configuration at zero magnetic field below the magnetic ordering temperature of the material.<sup>[123]</sup>



In the helimagnetic state, neighboring moments twist with a certain chirality, left-handed or right-handed, in the plane perpendicular to the propagation axis, which lies typically along a crystallographic or high symmetry direction. The twisting occurs as a consequence of the chiral crystal structure which lacks inversion symmetry enforcing the antisymmetric Dzyaloshinskii–Moriya interaction, resulting in long-period helical spin modulations. In the presence of external magnetic fields, the helimagnetic state, depending on the crystalline structure and anisotropy, can transform into a range of nontrivial magnetic states, comprising most commonly of the conical state,<sup>[126]</sup> tilted conical state,<sup>[127]</sup> the 1D soliton lattice state,<sup>[128]</sup> as well as the 2D topological skyrmion lattice state.<sup>[129]</sup>

Within the family of bulk chiral magnets, the most extensively studied has been that of MnSi, as this was the first compound identified experimentally to host topological skyrmions in applied fields near the helimagnetic to paramagnetic transition.<sup>[129]</sup> Following this discovery, the field of noncollinear magnetism underwent a renaissance of research activity, and today the creation and annihilation of skyrmions as well as their motion under electric currents has been well documented. Here, Hall measurements revealed a depinning of skyrmions from impurities at current densities as low as  $10^6 \text{ A m}^{-2}$ ,<sup>[130]</sup> which is orders of magnitude less than the densities required to induce motion of FM domain walls. As a result, this has fuelled great interest in the development of new information storage, logic, and quantum computation devices which utilize skyrmions.

Consequently, current research is focused on resolving the magnetic order of chiral magnets prepared as thin films. Finite-size effects and symmetry breaking at thin-film interfaces are expected to modify the ground state magnetic configuration of chiral magnets, leading to alternate forms of magnetic order which are not stabilized in the bulk crystal. In thin films exhibiting helimagnetic order, the propagation direction is most commonly found to lie along the film normal, with the moments lying in the film plane and aligning ferromagnetically at each given depth.<sup>[131–135]</sup> As the magnetization varies as a function of film depth over the helical wavelength  $\lambda_h$ , and the moments lie in the plane of the film, PNR is an ideal technique to investigate the spin order, where the analysis of SA data allows easy detection and depth-profiling of the in-plane helical moments.

Early PNR measurements performed on epitaxial MnSi with a thickness of  $t = 39.5 \text{ nm}$  revealed a helical magnetic order with  $\lambda_h = 13.9 \text{ nm}$  propagating along the film normal.<sup>[131]</sup> The distinct change in the magnetic order of the epitaxial film compared to bulk MnSi was explained to arise from the in-plane uniaxial anisotropy induced by the epitaxial strain at the interface to the thin film substrate.<sup>[132]</sup> PNR data collected with full spin analysis were used to conclude that the film consisted of both left-handed and right-handed chiral structures in equal fractions because  $R^{+-} = R^{-+}$ , resulting in a depth-dependent magnetization profile consistent with a superposition of left-handed and right-handed spin-density waves. Additional modeling revealed that the handedness of a single domain chiral magnet would manifest itself as a Bragg peak in only one of the spin channels,<sup>[132]</sup> where a right-handed helix would produce a peak in the  $R^{+-}$  channel, while a left-handed helix would produce a

Bragg peak in the  $R^{-+}$  channel, essentially allowing phase information of the magnetic order to be determined.

Continued work on epitaxial MnSi with thickness  $t = 26.7 \text{ nm}$  established that the helical wavelength was independent of the film thickness, remaining at a constant value of  $\lambda_h = 13.9 \text{ nm}$  for film thicknesses between  $t = 7$  and  $40 \text{ nm}$ .<sup>[133]</sup> Through a detailed PNR investigation, it was revealed that the magnetic order comprised of confined helicoids which unwound via discrete steps in the presence of external magnetic fields, as depicted in **Figure 7a**. Here, SA information encoded in the difference between the  $R^{++}$  and  $R^{--}$  data was crucial to revealing the field-dependent magnetization profiles of the out-of-plane propagating helical order of the film at each corresponding value of the external magnetic field. As shown in **Figure 7b**, the SA and corresponding magnetization profile of the MnSi film was found to unwind from a two-twist state at low fields (i.e.,  $B = 32 \text{ mT}$ ), to a one-twist state at intermediate fields (i.e.,  $B = 200\text{--}400 \text{ mT}$ ) and finally into to a forced FM state at high fields (i.e.,  $B = 700 \text{ mT}$ ). These results were later corroborated by several additional and independent PNR and small-angle neutron scattering investigations into the magnetic order of epitaxial FeGe,<sup>[135,136]</sup>  $\text{Fe}_{1-x}\text{Co}_x\text{Si}$ ,<sup>[137]</sup> and  $\text{Fe}_{1-x}\text{Co}_x\text{Ge}$ ,<sup>[138]</sup> which were found to comprise of an integer number of out-of-plane propagating helical wavelengths which unwound in the presence of an external magnetic field. Finite size effects present in the epitaxial films were determined to be responsible for the observed quantization of helicoidal turns, and it was further demonstrated that the number of helicoidal turns could be “read out” by electrical transport measurements.

A PNR investigation by Meynell et al. on epitaxial MnSi with a thickness  $t = 26.7 \text{ nm}$  concluded the observation of in-plane skyrmions.<sup>[139]</sup> These findings seemingly contradict the earlier work described in ref. [133] for measurements performed on the exact same film. These two contradictory results highlight some of the difficulties of analyzing PNR data, which requires the assumption of complex scattering profiles with several independent parameters, and from this, the possibility to obtain non-unique fitting solutions.

A further practical limitation of PNR for the study of chiral spin systems is that PNR averages in-plane structure along the  $x$ -direction, due to relaxed beam collimation. This prevents  $Q_x$  resolution in the plane of the film which limits the ability of the PNR technique to simultaneously provide resolution in  $Q_x$  and  $Q_y$  needed to resolve complex lateral correlations.<sup>[140]</sup> As such, reflectometry alone is not able to provide sufficient angular resolution to fully resolve lateral correlations such as in-plane or out-of-plane skyrmion lattices. To overcome this limitation, comprehensive neutron scattering investigations employing not only specular and off-specular PNR, but also near-surface small angle neutron scattering,<sup>[141]</sup> are required to resolve all three  $Q$  directions (i.e.,  $Q_x$ ,  $Q_y$  and  $Q_z$ ) for full phase space determination on a single film.<sup>[134]</sup>

An intriguing subset of chiral magnets where the Dzyaloshinskii–Moriya interaction is not an innate property of the crystal structure, but rather artificially generated through thin film engineering, is that of heterostructures consisting of FM and heavy metal layers. In such systems, the Dzyaloshinskii–Moriya interaction results from the breaking of inversion symmetry at the interfaces which provides a strong spin–orbit



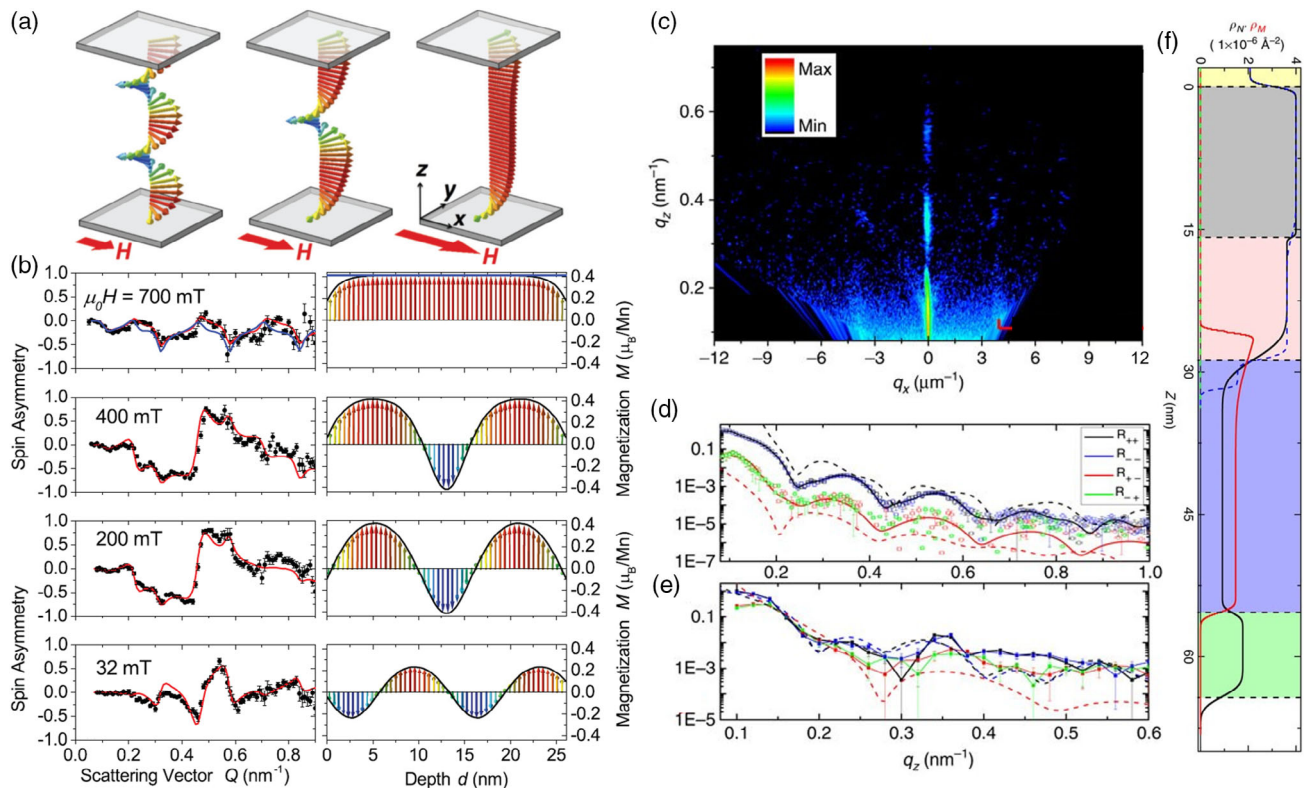


**Figure 7.** Key role of PNR for the study of chiral spin systems. a) Schematic of the field-induced unwinding of helical moments in epitaxial MnSi with  $t = 26.7$  nm. b) Measured (black circles) and calculated (red line) SA for epitaxial MnSi at  $T = 5$  K and  $B = 700, 400, 200,$  and  $32$  mT and the corresponding magnetic SLD profiles. Reproduced with permission.<sup>[133]</sup> Copyright 2013, American Physical Society. c) Position-sensitive area detector image of scattering from a Co nanodot array grown on Co/Pd. d) Specular and e) off-specular scattering profiles and the f) corresponding nuclear and magnetic SLD profile of the Co nanodot array grown on Co/Pd. Reproduced under the terms of the CC-BY 4.0 License.<sup>[145]</sup> Copyright 2015, The Authors. Published by Springer Nature Limited.

coupling leading to a Dzyaloshinskii–Moriya interaction with a similar magnitude to the Heisenberg exchange.<sup>[142]</sup> Early pioneering works on ultrathin epitaxial films ultimately showed that skyrmion lattice states could be achieved in 1 ML Fe on Ir(111),<sup>[143]</sup> albeit at temperatures well below those required for everyday applications. A proven approach to enhance the thermal stability of the skyrmion lattice is to grow heterostructure stacks comprised of multiple repetitions of thin FM and heavy metal layers by sputter deposition.<sup>[142,144]</sup> To this end, a recent PNR investigation on in-plane easy axis Co nanodot arrays grown on Co/Pd underlayers with perpendicular magnetic anisotropy, reported the observation of room-temperature skyrmions at ambient pressure in the absence of external magnetic fields.<sup>[145]</sup> As shown in Figure 7c, a position-sensitive area detector was used to simultaneously collect both specular (Figure 7d) and off-specular (Figure 7e) PNR data on the Co nanodot arrays. From the extracted SLD profile shown in Figure 7f, the authors were able to confirm the imprinting of an artificial Bloch-type skyrmion lattice into the Co/Pd film in the regions beneath the Co nanodot arrays. These artificially constructed skyrmion lattice arrays, which are controlled by exchange and magneto-static interactions, demonstrate an exciting new platform to use PNR to explore room-temperature ground-state skyrmion lattices in the future.

## 4. Conclusion and Outlook

The coming decades are rich with possibilities to deploy PNR to optimize quantum materials and heterostructures, and this field is rapidly expanding. It is anticipated that practical quantum technologies will not simply exploit a single material, but, analogous to semiconductor fabrication, will combine dozens of separate materials into a complex “stack” to deliver the desired functionality. In this context, the role of interfaces and heterostructures will become increasingly important. With the innate depth-sensitivity of PNR, the technique is able to reveal buried features, thus offering some capabilities not afforded by pure surface science probes such as ARPES or STM. This may increasingly come to the forefront as quantum technology evolves into more complex 3D nanoarchitectures.

The ability to nondestructively study materials during different stages of device processing and under a variety of environments (e.g., temperature, magnetic field, pressure, atmosphere) should enable PNR to become a useful technique to study device processing conditions that are necessary to bring quantum technology into our everyday reality. In particular, the ability to track hydrogen gas and moisture content in films and correlate this with superconducting, electrical, or magnetic performance may become critical. In situ transport measurements,<sup>[98]</sup>

and other device modalities such as FM resonance,<sup>[87]</sup> are expected to increasingly feature on state-of-the-art PNR beamlines as complementary ancillary measurements.

In the short-term there are great opportunities to use PNR to study the type of junctions relevant to transmon qubit architectures based on classical superconductors, and this field to date, seems to be heavily underexplored; however, it is well within the capabilities of current generation PNR beamlines.

In the vast field of TMO interfaces, different trends are arising to achieve new functionalities for applications. In particular, there is increased interest in the so-called Mottronics, which are based on the ability to switch a material from a Mott insulator to a metallic state. This has been realized via hydrogen-induced electron doping in several correlated perovskite materials.<sup>[146]</sup> Devices based on this concept are perfect candidates for PNR studies combined with in situ transport measurements, in which a given resistive state can be correlated with depth-dependent hydrogen and magnetic profiling.

There is currently a substantial opportunity to expand the study of magnetic topological phases. The study of magnetic TIs and proximity effects is expected to grow from the strong existing foundation. Future work will likely explore other topological phases including Dirac and Weyl semimetals. Another underexplored area is that of topological superconductors which are a platform for error-resistant quantum computing based on Majorana fermions. However, given the low critical temperatures, improvements in in situ dilution refrigeration for PNR instrumentation is a key requirement to explore this area.

The integration of complex magnetic structures, such as chiral spin systems and skyrmion textures, into quantum technology “stacks” is expected to add further functionality to devices through the additional degrees of freedom of topology and chirality. In this area, the prevalence of grazing-incidence neutron diffraction or near-surface small-angle neutron scattering studies are anticipated to increase as the desire to resolve complex in-plane magnetic correlations continues to strengthen.<sup>[141]</sup> A current untapped area appears to be PNR investigations of the monoaxial chiral magnets, which are structures that generally comprise of 1D topological magnetic soliton lattices making them ideal textures to study using PNR. One limitation, however, is the dynamic nature of solitons, and as such, rapid PNR counting times would be required to avoid measuring the time-averaged solitonic structure.

Intensive studies on 2D materials, such as graphene,<sup>[147]</sup> are expected to emerge as better neutron instrumentation becomes available. In particular, high brilliance neutron sources such as the 5 MW source currently under construction at the European Spallation Source (ESS) in Sweden,<sup>[148]</sup> and improved instrument designs,<sup>[149]</sup> will deliver higher focusing and signal-to-noise ratios required to measure smaller samples to higher  $Q$ , and therefore resolve thinner layers in the range of 0.3–1 nm.

Improvements in thin film deposition will also broaden the applicability of PNR to new classes of quantum materials. For example, there have been relatively few thin film studies of heavy fermion systems, despite these being extensively explored in bulk. As atomically flat films and surfaces become available,<sup>[150]</sup> PNR will become increasingly applicable to these novel quantum materials.

The growing ability to conduct PNR in vacuum deposition systems will also allow the technique to progressively expand into the pure surface science regime.<sup>[151]</sup> Despite their immense value as a structural and magnetic probe, neutrons are not ideal for probing electronic structures, which are an essential aspect in advanced electronic materials. Therefore, we anticipate a growing number of studies combining PNR with electronic surface measurement techniques such as ARPES and STM. Furthermore, as small-scale “lab versions” of these techniques do exist, it is possible to envision full-feature beamlines in the future that combine multiple capabilities along with PNR for “full stack” quantum materials characterization.

## Acknowledgements

The authors acknowledge the Helmholtz-Zentrum Berlin, the Heinz Maier-Leibnitz Zentrum, and the Australian Nuclear Science and Technology Organisation (under proposals P5062, P5351, P5808, P6196, and P6223) for the provision of neutron beamtime. This work has been funded by the Deutsche Forschungsgemeinschaft (DFG, German Research Foundation) under TRR80 (From Electronic Correlations to Functionality, Project No. 107745057, Project F7), the priority program SPP 2137 (Skyrmionics) under grant PF393/19 (project-id 403191981), the excellence cluster MCQST under Germany's Excellence Strategy EXC-2111 (Project No. 390814868), the Australian Government and the Australian Research Council Centre of Excellence in Future Low Energy Electronics Technologies (project no. 8CE170100039). D.C. acknowledges the support of an Australian Research Council Fellowship DE180100314. Open Access funding enabled and organized by Projekt DEAL.

## Conflict of Interest

The authors declare no conflict of interest.

## Keywords

chiral magnets, hydrogen, neutron scattering, superconductors, thin film interfaces, topological materials, transition metal oxide interfaces

Received: October 31, 2022

Revised: December 8, 2022

Published online: January 19, 2023

- [1] F. Giustino, J. H. Lee, F. Trier, M. Bibes, S. M. Winter, R. Valentí, Y.-W. Son, L. Taillefer, C. Heil, A. I. Figueroa, B. Plaçais, Q. Wu, O. V. Yazyev, E. P. A. M. Bakkers, J. Nygård, P. Forn-Díaz, S. D. Franceschi, J. W. McIver, L. E. F. Torres, T. Low, A. Kumar, R. Galceran, S. O. Valenzuela, M. V. Costache, A. Manchon, E.-A. Kim, G. R. Schleder, A. Fazzio, S. Roche, *J. Phys.: Mater.* **2020**, *3*, 042006.
- [2] CSIRO, Growing Australia's Quantum Industry, <https://www.csiro.au/en/work-with-us/services/consultancy-strategic-advice-services/csiro-futures/future-industries/quantum> **2021** (accessed: July 2022).
- [3] F. Arute, K. Arya, R. Babbush, D. Bacon, J. C. Bardin, R. Barends, R. Biswas, S. Boixo, F. G. S. L., D. A. Buell, B. Burkett, Y. Chen, Z. Chen, B. Chiaro, R. Collins, W. Courtney, A. Dunsworth, E. Farhi, B. Foxen, A. Fowler, C. Gidney, M. Giustina, R. Graff, K. Guerin, S. Habegger, M. P. Harrigan, M. J. Hartmann, A. Ho, M. Hoffmann, T. Huang, et al., *Nature* **2019**, *574*, 505.

- [4] H. Y. Hwang, Y. Iwasa, M. Kawasaki, B. Keimer, N. Nagaosa, Y. Tokura, *Nat. Mater.* **2012**, *11*, 103.
- [5] J. Ankner, G. Felcher, *J. Magn. Magn. Mater.* **1999**, *200*, 741.
- [6] E. Dagotto, Y. Tokura, *MRS Bull.* **2008**, *33*, 1037.
- [7] C. Back, V. Cros, H. Ebert, K. Everschor-Sitte, A. Fert, M. Garst, T. Ma, S. Mankovsky, T. L. Monchesky, M. Mostovoy, N. Nagaosa, S. S. P. Parkin, C. Pfleiderer, N. Reyren, A. Rosch, Y. Taguchi, Y. Tokura, K. von Bergmann, J. Zang, *J. Phys. D: Appl. Phys.* **2020**, *53*, 363001.
- [8] E. Y. Vedmedenko, R. K. Kawakami, D. D. Sheka, P. Gambardella, A. Kirilyuk, A. Hirohata, C. Binek, O. Chubykalo-Fesenko, S. Sanvito, B. J. Kirby, J. Grollier, K. Everschor-Sitte, T. Kampfrath, C.-Y. You, A. Berger, *J. Phys. D: Appl. Phys.* **2020**, *53*, 453001.
- [9] S. J. Callori, T. Saerbeck, D. L. Cortie, K.-W. Lin, in *Solid State Physics*, (Ed: R. L. Stamps), Vol. 71, Academic Press, San Diego, United States **2020**, Ch. 3, pp. 73–116.
- [10] A. J. Grutter, Q. L. He, *Phys. Rev. Mater.* **2021**, *5*, 090301.
- [11] A. I. Figueroa, T. Hesjedal, N.-J. Steinke, *Appl. Phys. Lett.* **2020**, *117*, 150502.
- [12] E. Fermi, W. H. Zinn, *Reflection of Neutrons on Mirrors*, MDCC 56, U.S. Atomic Energy Commission, Los Alamos National Laboratory, Oak Ridge, Tennessee: Manhattan District **1946**, [https://books.google.com.au/books?id=IKsY9gzauUC&printsec=frontcover&source=gbs\\_ge\\_summary\\_r&cad=0#v=onepage&q&f=false](https://books.google.com.au/books?id=IKsY9gzauUC&printsec=frontcover&source=gbs_ge_summary_r&cad=0#v=onepage&q&f=false).
- [13] E. Fermi, L. Marshall, *Phys. Rev.* **1947**, *71*, 666.
- [14] D. J. Hughes, M. T. Burgy, *Phys. Rev.* **1951**, *81*, 498.
- [15] J. B. Hayter, J. Penfold, W. G. Williams, *Nature* **1976**, *262*, 569.
- [16] J. B. Hayter, J. Penfold, *J. Chem. Soc., Faraday Trans. 1* **1981**, *77*, 1851.
- [17] G. P. Felcher, *Phys. Rev. B* **1981**, *24*, 1595.
- [18] J. Penfold, R. C. Ward, W. G. Williams, *J. Phys. E: Sci. Instrum.* **1987**, *20*, 1411.
- [19] G. P. Felcher, R. O. Hilleke, R. K. Crawford, J. Haumann, R. Kleb, G. Ostrowski, *Rev. Sci. Instrum.* **1987**, *58*, 609.
- [20] A. T. Boothroyd, *Principles of Neutron Scattering from Condensed Matter*, 1st ed., Oxford University Press, Oxford, UK **2020**.
- [21] C. F. Majkrzak, *Physica B* **1991**, *173*, 75.
- [22] T. Chatterji, *Neutron Scattering from Magnetic Materials*, Elsevier, Amsterdam, Netherlands **2006**.
- [23] F. Ott, *JDN* **2014**, *13* 02004.
- [24] B. P. Toperverg, H. Zabel, in *Experimental Methods in the Physical Sciences*, (Eds: F. Fernandez-Alonso, D. L. Price), Vol. 48, Academic Press, London, United Kingdom **2015**, Ch. 6, 339–434.
- [25] C. F. Majkrzak, J. Penfold, *Neutron News* **2010**, *21*, 46.
- [26] J. F. Ankner, G. P. Felcher, *J. Magn. Magn. Mater.* **1999**, *200*, 741.
- [27] C. Majkrzak, *Physica B* **1996**, *221*, 342.
- [28] P. A. Kienzle, B. B. Maranville, K. V. O'Donovan, J. F. Ankner, C. F. Majkrzak, *Reflectometry Software* **2017**, <https://www.nist.gov/ncnr/data-reduction-analysis/reflectometry-software> (accessed: October 2022).
- [29] A. J. Nelson, S. Prescott, *J. Appl. Crystallogr.* **2019**, *52*, 193.
- [30] M. Björck, G. Andersson, *J. Appl. Crystallogr.* **2007**, *40*, 1174.
- [31] G. Pospelov, W. Van Herck, J. Burle, J. M. Carmona Loaiza, C. Durniak, J. M. Fisher, M. Ganeva, D. Yurov, J. Wuttke, *J. Appl. Crystallogr.* **2020**, *53*, 262.
- [32] G. P. Felcher, R. T. Kampwirth, K. E. Gray, R. Felici, *Phys. Rev. Lett.* **1984**, *52*, 1539.
- [33] H. Zhang, J. W. Lynn, C. F. Majkrzak, S. K. Satija, J. H. Kang, X. D. Wu, *Phys. Rev. B* **1995**, *52*, 10395.
- [34] A. A. Murthy, P. Masih Das, S. M. Ribet, C. Kopas, J. Lee, M. J. Reagor, L. Zhou, M. J. Kramer, M. C. Hersam, M. Checchin, A. Grassellino, R. D. Reis, V. P. Dravid, A. Romanenko, *ACS Nano* **2022**, *16*, 17257.
- [35] A. Costa, M. Sutula, V. Lauter, J. Song, J. Fabian, J. S. Moodera, *New J. Phys.* **2022**, *24*, 033046.
- [36] C. Müller, J. H. Cole, J. Lisenfeld, *Rep. Prog. Phys.* **2019**, *82*, 124501.
- [37] J. Stahn, J. Chakhalian, C. Niedermayer, J. Hoppler, T. Gutberlet, J. Voigt, F. Treubel, H.-U. Habermeier, G. Cristiani, B. Keimer, C. Bernhard, *Phys. Rev. B* **2005**, *71*, 140509.
- [38] J. Chakhalian, J. W. Freeland, G. Srajer, J. Stremper, G. Khaliullin, J. C. Cezar, T. Charlton, R. Dalgliesh, C. Bernhard, G. Cristiani, H.-U. Habermeier, B. Keimer, *Nat. Phys.* **2006**, *2*, 244.
- [39] J. Hoppler, J. Stahn, C. Niedermayer, V. K. Malik, H. Bouyanff, A. J. Drew, M. Rössle, A. Buzdin, G. Cristiani, H.-U. Habermeier, B. Keimer, C. Bernhard, *Nat. Mater.* **2009**, *8*, 315.
- [40] J. Hoppler, H. Fritzsche, V. K. Malik, J. Stahn, G. Cristiani, H.-U. Habermeier, M. Rössle, J. Honolka, A. Enders, C. Bernhard, *Phys. Rev. B* **2010**, *82*, 174439.
- [41] C. Visani, J. Tornos, N. M. Nemes, M. Rocci, C. Leon, J. Santamaria, S. G. E. te Velthuis, Y. Liu, A. Hoffmann, J. W. Freeland, M. Garcia-Hernandez, M. R. Fitzsimmons, B. J. Kirby, M. Varela, S. J. Pennycook, *Phys. Rev. B* **2011**, *84*, 060405.
- [42] Y. Liu, C. Visani, N. M. Nemes, M. R. Fitzsimmons, L. Y. Zhu, J. Tornos, M. Garcia-Hernandez, M. Zhernenkov, A. Hoffmann, C. Leon, J. Santamaria, S. G. E. te Velthuis, *Phys. Rev. Lett.* **2012**, *108*, 207205.
- [43] J. Chakhalian, J. W. Freeland, G. E. A. Srajer, *Nat. Phys.* **2006**, *2*, 244.
- [44] M. A. Uribe-Laverde, D. K. Satapathy, I. Marozau, V. K. Malik, S. Das, K. Sen, J. Stahn, A. Rühm, J.-H. Kim, T. Keller, A. Devishvili, B. P. Toperverg, C. Bernhard, *Phys. Rev. B* **2013**, *87*, 115105.
- [45] R. de Andrés Prada, R. Gaina, N. Biškup, M. Varela, J. Stahn, C. Bernhard, *Phys. Rev. B* **2019**, *100*, 115129.
- [46] H. Bhatt, Y. Kumar, C. L. Prajapat, C. J. Kinane, A. Caruana, S. Langridge, S. Basu, S. Singh, *ACS Appl. Mater. Interfaces* **2022**, *14*, 8565.
- [47] Y. N. Khaydukov, B. Nagy, J.-H. Kim, T. Keller, A. Rühm, Y. V. Nikitenko, K. N. Zhernenkov, J. Stahn, L. F. Kiss, A. Csik, L. Bottyán, V. L. Aksenov, *JETP Lett.* **2013**, *98*, 107.
- [48] F. Radu, V. Ignatovich, *Physica B* **2000**, *292*, 160.
- [49] C. L. Prajapat, S. Singh, D. Bhattacharya, G. Ravikumar, S. Basu, S. Matthauch, J.-G. Zheng, T. Aoki, A. Paul, *Sci. Rep.* **2018**, *8*, 3732.
- [50] O. H. C. Paull, A. V. Pan, G. L. Causer, S. A. Fedoseev, A. Jones, X. Liu, A. Rosenfeld, F. Klose, *Nanoscale* **2018**, *10*, 18995.
- [51] Y. Kumar, H. Bhatt, C. L. Prajapat, A. P. Singh, F. Singh, C. J. Kinane, S. Langridge, S. Basu, S. Singh, *J. Appl. Phys.* **2021**, *129*, 163902.
- [52] M. Vaughan, N. Satchell, M. Ali, C. J. Kinane, G. B. G. Stenning, S. Langridge, G. Burnell, *Phys. Rev. Res.* **2020**, *2*, 013270.
- [53] D. I. Khomskii, *Transition Metal Compounds*, Cambridge University Press, Cambridge, United Kingdom **2014**.
- [54] H. Hwang, Y. Iwasa, M. Kawasaki, B. Keimer, N. Nagaosa, Y. Tokura, *Nat. Mater.* **2012**, *11*, 103.
- [55] J. Mannhart, D. G. Schlom, *Science* **2010**, *327*, 1607.
- [56] M. Coll, J. Fontcuberta, M. Althammer, M. Bibes, H. Boschker, A. Calleja, G. Cheng, M. Cuoco, R. Dittmann, B. Dkhil, I. El Baggari, M. Fanciulli, I. Fina, E. Fortunato, C. Frontera, S. Fujita, V. Garcia, S. T. B. Goennenwein, C. G. Granqvist, J. Grollier, R. Gross, A. Hagfeldt, G. Herranz, K. Hono, E. Houwman, M. Huijben, A. Kalaboukhov, D. J. Keeble, G. Koster, L. F. Kourkoutis, et al. *Appl. Surf. Sci.* **2019**, *482*, 1.
- [57] M. Bibes, A. Barthelemy, *IEEE Trans. Electron Devices* **2007**, *54*, 1003.
- [58] Y. Liu, X. Ke, *J. Phys.: Condens. Matter* **2015**, *27*, 373003.
- [59] E. Benckiser, Y. Khaydukov, L. Guasco, K. Fürsich, P. Radhakrishnan, G. Kim, B. Keimer, *Phys. Status Solidi B* **2022**, *259*, 2100253.
- [60] C. He, A. J. Grutter, M. Gu, N. D. Browning, Y. Takamura, B. J. Kirby, J. A. Borchers, J. W. Kim, M. R. Fitzsimmons, X. Zhai, V. V. Mehta, F. J. Wong, Y. Suzuki, *Phys. Rev. Lett.* **2012**, *109*, 197202.



- [61] A. J. Grutter, H. Yang, B. J. Kirby, M. R. Fitzsimmons, J. A. Aguiar, N. D. Browning, C. A. Jenkins, E. Arenholz, V. V. Mehta, U. S. Alaan, Y. Suzuki, *Phys. Rev. Lett.* **2013**, *111*, 087202.
- [62] A. Bhattacharya, S. J. May, S. G. E. te Velthuis, M. Warusawithana, X. Zhai, B. Jiang, J.-M. Zuo, M. R. Fitzsimmons, S. D. Bader, J. N. Eckstein, *Phys. Rev. Lett.* **2008**, *100*, 257203.
- [63] J. Hemberger, A. Krimmel, T. Kurz, H.-A. Krug von Nidda, V. Y. Ivanov, A. A. Mukhin, A. M. Balbashov, A. Loidl, *Phys. Rev. B* **2002**, *66*, 094410.
- [64] A. Glavic, H. Dixit, V. R. Cooper, A. A. Aczel, *Phys. Rev. B* **2016**, *93*, 140413.
- [65] M. Keunecke, F. Lyzwa, D. Schwarzbach, V. Roddatis, N. Gauquelin, K. Müller-Caspary, J. Verbeeck, S. J. Callori, F. Klose, M. Jungbauer, V. Moshnyaga, *Adv. Funct. Mater.* **2020**, *30*, 1808270.
- [66] S. J. May, A. B. Shah, S. G. E. te Velthuis, M. R. Fitzsimmons, J. M. Zuo, X. Zhai, J. N. Eckstein, S. D. Bader, A. Bhattacharya, *Phys. Rev. B* **2008**, *77*, 174409.
- [67] T. S. Santos, B. J. Kirby, S. Kumar, S. J. May, J. A. Borchers, B. B. Maranville, J. Zarestky, S. G. E. te Velthuis, J. van den Brink, A. Bhattacharya, *Phys. Rev. Lett.* **2011**, *107*, 167202.
- [68] J. Zhang, J. Yang, G. L. Causer, J. Shi, F. Klose, J.-K. Huang, A. Tseng, D. Wang, X. Zu, L. Qiao, A. Pham, S. Li, *Phys. Rev. B* **2021**, *104*, 174444.
- [69] G. Kim, Y. Khaydukov, M. Bluschke, Y. E. Suyolcu, G. Christiani, K. Son, C. Dietl, T. Keller, E. Weschke, P. A. van Aken, G. Logvenov, B. Keimer, *Phys. Rev. Mater.* **2019**, *3*, 084420.
- [70] G. A. Ovsyannikov, T. A. Shaikhulov, K. L. Stankevich, Y. Khaydukov, N. V. Andreev, *Phys. Rev. B* **2020**, *102*, 144401.
- [71] E.-J. Guo, M. A. Roldan, X. Sang, S. Okamoto, T. Charlton, H. Ambaye, H. N. Lee, M. R. Fitzsimmons, *Phys. Rev. Mater.* **2018**, *2*, 114404.
- [72] C. Liu, Y. Liu, B. Zhang, C.-J. Sun, D. Lan, P. Chen, X. Wu, P. Yang, X. Yu, T. Charlton, M. R. Fitzsimmons, J. Ding, J. Chen, G. M. Chow, *ACS Appl. Mater. Interfaces* **2021**, *13*, 30137.
- [73] C. L. Prajapat, H. Bhatt, Y. Kumar, T. V. C. Rao, P. K. Mishra, G. Ravikumar, C. J. Kinane, B. Satpati, A. Caruana, S. Langridge, S. Basu, S. Singh, *ACS Appl. Electron. Mater.* **2020**, *2*, 2629.
- [74] J.-H. Kim, I. Vrejoiu, Y. Khaydukov, T. Keller, J. Stahn, A. Rühm, D. K. Satapathy, V. Hinkov, B. Keimer, *Phys. Rev. B* **2012**, *86*, 180402.
- [75] A. M. Kane, I.-T. Chiu, N. J. Ahlm, R. V. Chopdekar, A. T. N'Diaye, E. Arenholz, A. Mehta, V. Lauter, Y. Takamura, *ACS Appl. Mater. Interfaces* **2020**, *12*, 45437.
- [76] J. D. Hoffman, B. J. Kirby, J. Kwon, G. Fabbris, D. E. A. Meyers, *Phys. Rev. X* **2016**, *6*, 041038.
- [77] B. Chen, H. Xu, C. Ma, S. Mattauch, D. Lan, F. Jin, Z. Guo, S. Wan, P. Chen, G. Gao, F. Chen, Y. Su, W. Wu, *Science* **2017**, *357*, 191.
- [78] S. G. Jeong, J. Kim, A. Seo, S. Park, H. Y. Jeong, Y.-M. Kim, V. Lauter, T. Egami, J. H. Han, W. S. Choi, *Sci. Adv.* **2022**, *8*, eabm4005.
- [79] L. Guasco, Y. Khaydukov, G. Kim, T. Keller, A. Vorobiev, A. Devishvili, P. Wochner, G. Christiani, G. Logvenov, B. Keimer, *Adv. Mater.* **2022**, *34*, 2202971.
- [80] V. Leiner, K. Westerholt, B. Hj Rvarsson, H. Zabel, *J. Phys. D: Appl. Phys.* **2002**, *35*, 2377.
- [81] B. Hjörvarsson, J. A. Dura, P. Isberg, T. Watanabe, T. J. Udovic, G. Andersson, C. F. Majkrzak, *Phys. Rev. Lett.* **1997**, *79*, 901.
- [82] F. Klose, C. Rehm, D. Nagengast, H. Maletta, A. Weidinger, *Phys. Rev. Lett.* **1997**, *78*, 1150.
- [83] E. Kravtsov, A. Nefedov, G. Nowak, K. Zhernenkov, H. Zabel, B. Hjörvarsson, A. Liebig, A. Hoser, G. J. McIntyre, L. Paolasini, A. Remhof, *J. Phys.: Condens. Matter* **2009**, *33*, 336004.
- [84] S. Watt, M. Kostylev, *Phys. Rev. B* **2020**, *101*, 174422.
- [85] P. Chang, T. Chuang, D. Wei, W. Lin, *Appl. Phys. Lett.* **2020**, *116*, 102407.
- [86] A. J. Tan, M. Huang, C. O. Avci, F. Büttner, M. Mann, W. Hu, C. Mazzoli, S. Wilkins, H. L. Tuller, G. S. D. Beach, *Nat. Mater.* **2019**, *18*, 35.
- [87] G. L. Causer, M. Kostylev, D. L. Cortie, C. Lueng, S. J. Callori, X. L. Wang, F. Klose, *ACS Appl. Mater. Interfaces* **2019**, *11*, 35420.
- [88] J. Shi, Y. Zhou, S. Ramanathan, *Nat. Commun.* **2014**, *5*, 4860.
- [89] J. Chen, Y. Zhou, S. Middey, J. Jiang, N. Chen, L. Chen, X. Shi, M. Döbeli, J. Shi, J. Chakhalian, S. Ramanathan, *Appl. Phys. Lett.* **2015**, *1073*, 031905.
- [90] C. Oh, S. Heo, H. M. Jang, J. Son, *Appl. Phys. Lett.* **2016**, *108*, 122106.
- [91] Y. Cui, G. Zhang, H. Li, H. Lin, X. Zhu, H. Wen, G. Wang, J. Sun, M. Ma, Y. Li, D. Gong, T. Xie, Y. Gu, S. Li, H. Luo, P. Yu, W. Yu, *Sci. Bull.* **2018**, *63*, 11.
- [92] D. Li, K. Lee, B. Wang, M. Osada, S. Crossley, H. Lee, Y. Cui, Y. Hikita, H. Hwang, *Nature* **2019**, *572*, 624.
- [93] L. Si, W. Xiao, J. Kaufmann, J. M. Tomczak, Y. Lu, Z. Zhong, K. Held, *Phys. Rev. Lett.* **2020**, *124*, 166402.
- [94] S. J. Callori, C. Rehm, G. L. Causer, M. Kostylev, F. Klose, *Metals* **2016**, *6*, 125.
- [95] J. Lee, Y. Ha, S. Lee, *Adv. Mater.* **2021**, *33*, 2007606.
- [96] A. R. Mazza, Q. Lu, G. Hu, H. Li, J. F. Browning, T. R. Charlton, M. Brahlek, P. Ganesh, T. Z. Ward, H. N. Lee, G. Eres, *ACS Appl. Mater. Interfaces* **2022**, *14*, 10898.
- [97] K. Munbodh, F. A. Perez, C. Keenan, D. Lederman, M. Zhernenkov, M. R. Fitzsimmons, *Phys. Rev. B* **2011**, *83*, 094432.
- [98] L. Guasco, Y. N. Khaydukov, S. Pütter, L. Silvi, M. Paulin, T. Keller, B. Keimer, *Nat. Commun.* **2022**, *13*, 1486.
- [99] M. Wolff, A. Devishvili, J. A. Dura, F. A. Adlmann, B. Kitchen, G. K. Pálsson, H. Palonen, B. B. Maranville, C. F. Majkrzak, B. P. Toperverg, *Phys. Rev. Lett.* **2019**, *123*, 016101.
- [100] A. Perrichon, A. Devishvili, K. Komander, G. K. Pálsson, A. Vorobiev, R. Lavén, M. Karlsson, M. Wolff, *Phys. Rev. B* **2021**, *103*, 235423.
- [101] R. Moessner, J. E. Moore, *Topological Phases of Matter*, Cambridge University Press, Cambridge, United Kingdom **2021**.
- [102] C.-Z. Chang, J. Zhang, X. Feng, J. Shen, Z. Zhang, M. Guo, K. Li, Y. Ou, P. Wei, L.-L. Wang, Z.-Q. Ji, Y. Feng, S. Ji, X. Chen, J. Jia, X. Dai, Z. Fang, S.-C. Zhang, K. He, Y. Wang, L. Lu, X.-C. Ma, Q.-K. Xue, *Science* **2013**, *340*, 167.
- [103] Y. Deng, Y. Yu, M. Z. Shi, Z. Guo, Z. Xu, J. Wang, X. H. Chen, Y. Zhang, *Science* **2020**, *367*, 895.
- [104] S. Bhattacharyya, G. Akhgar, M. Gebert, J. Karel, M. T. Edmonds, M. S. Fuhrer, *Adv. Mater.* **2021**, *33*, 2007795.
- [105] M. Li, C.-Z. Chang, B. J. Kirby, M. E. Jamer, W. Cui, L. Wu, P. Wei, Y. Zhu, D. Heiman, J. Li, J. S. Moodera, *Phys. Rev. Lett.* **2015**, *115*, 087201.
- [106] S. V. Eremeev, V. N. Men'shov, V. V. Tugushev, P. M. Echenique, E. V. Chulkov, *Phys. Rev. B* **2013**, *88*, 144430.
- [107] L. J. Collins-McIntyre, L. B. Duffy, A. Singh, N.-J. Steinke, C. J. Kinane, T. R. Charlton, A. Pushp, A. J. Kellock, S. S. P. Parkin, S. N. Holmes, C. H. W. Barnes, G. van der Laan, S. Langridge, T. Hesjedal, *EPL* **2016**, *115*, 27006.
- [108] L. B. Duffy, A. I. Figueroa, L. Gładczuk, N.-J. Steinke, K. Kummer, G. van der Laan, T. Hesjedal, *Phys. Rev. B* **2017**, *95*, 224422.
- [109] F. Katmis, V. Lauter, F. S. Nogueira, B. A. Assaf, M. E. Jamer, P. Wei, B. Satpati, J. W. Freeland, I. Eremin, D. Heiman, P. Jarillo-Herrero, J. S. Moodera, *Nature* **2016**, *533*, 513.
- [110] M. Li, Q. Song, W. Zhao, J. A. Garlow, T.-H. Liu, L. Wu, Y. Zhu, J. S. Moodera, M. H. W. Chan, G. Chen, C.-Z. Chang, *Phys. Rev. B* **2017**, *96*, 201301.
- [111] Q. L. He, X. Kou, A. J. Grutter, G. Yin, L. Pan, X. Che, Y. Liu, T. Nie, B. Zhang, S. M. Disseler, B. J. Kirby, W. Ratcliff II, Q. Shao,



- K. Murata, X. Zhu, G. Yu, Y. Fan, M. Montazeri, X. Han, J. A. Borchers, K. L. Wang, *Nat. Mater.* **2017**, *16*, 94.
- [112] L. B. Duffy, N.-J. Steinke, J. A. Krieger, A. I. Figueroa, K. Kummer, T. Lancaster, S. R. Giblin, F. L. Pratt, S. J. Blundell, T. Prokscha, A. Suter, S. Langridge, V. N. Strocov, Z. Salman, G. van der Laan, T. Hesjedal, *Phys. Rev. B* **2018**, *97*, 174427.
- [113] L. B. Duffy, N.-J. Steinke, D. M. Burn, A. Frisk, L. Lari, B. Kuerbanjiang, V. K. Lazarov, G. van der Laan, S. Langridge, T. Hesjedal, *Phys. Rev. B* **2019**, *100*, 054402.
- [114] Q. L. He, G. Yin, L. Yu, A. J. Grutter, L. Pan, C.-Z. Chen, X. Che, G. Yu, B. Zhang, Q. Shao, A. L. Stern, B. Casas, J. Xia, X. Han, B. J. Kirby, R. K. Lake, K. T. Law, K. L. Wang, *Phys. Rev. Lett.* **2018**, *121*, 096802.
- [115] Q. L. He, G. Yin, A. J. Grutter, L. Pan, X. Che, G. Yu, D. A. Gilbert, S. M. Disseler, Y. Liu, P. Shafer, B. Zhang, Y. Wu, B. J. Kirby, E. Arenholz, R. K. Lake, X. Han, K. L. Wang, *Nat. Commun.* **2018**, *9*, 2767.
- [116] C.-Y. Yang, L. Pan, A. J. Grutter, H. Wang, X. Che, Q. L. He, Y. Wu, D. A. Gilbert, P. Shafer, E. Arenholz, H. Wu, G. Yin, P. Deng, J. A. Borchers, W. Ratcliff, K. L. Wang, *Sci. Adv.* **2020**, *6*, eaaz8463.
- [117] N. Andrejevic, Z. Chen, T. Nguyen, L. Fan, H. Heiberger, L.-J. Zhou, Y.-F. Zhao, C.-Z. Chang, A. Grutter, M. Li, *Appl. Phys. Rev.* **2022**, *9*, 011421.
- [118] A. R. Mazza, J. Lapano, H. M. Meyer III, C. T. Nelson, T. Smith, Y.-Y. Pai, K. Noordhoek, B. J. Lawrie, T. R. Charlton, R. G. Moore, T. Z. Ward, M.-H. Du, G. Eres, M. Brahlek, *Adv. Funct. Mater.* **2022**, *32*, 2202234.
- [119] Y. Lv, J. Kally, T. Liu, P. Quarterman, T. Pillsbury, B. J. Kirby, A. J. Grutter, P. Sahu, J. A. Borchers, M. Wu, N. Samarth, J.-P. Wang, *Appl. Phys. Rev.* **2022**, *9*, 011406.
- [120] N. Bhattacharjee, K. Mahalingam, A. Fedorko, V. Lauter, M. Matzelle, B. Singh, A. Grutter, A. Will-Cole, M. Page, M. McConney, R. Markiewicz, A. Bansil, D. Heiman, N. X. Sun, *Adv. Mater.* **2022**, *34*, 2108790.
- [121] P. Deng, A. Grutter, Y. Han, M. E. Holtz, P. Zhang, P. Quarterman, S. Pan, S. Qi, Z. Qiao, K. L. Wang, *Nano Lett.* **2022**, *22*, 5735.
- [122] R. Akiyama, R. Ishikawa, K. Akutsu-Suyama, R. Nakanishi, Y. Tomohiro, K. Watanabe, K. Iida, M. Mitome, S. Hasegawa, S. Kuroda, *J. Phys. Chem. Lett.* **2022**, *13*, 8228.
- [123] A. Bauer, C. Pfleiderer, *Generic Aspects of Skyrmion Lattices in Chiral Magnets*, Springer International Publishing, Cham **2016**, pp. 1–28.
- [124] E. Ruff, S. Widmann, P. Lunkenheimer, V. Tsurkan, S. Bordács, I. Kézsmárki, A. Loidl, *Sci. Adv.* **2015**, *1*, 1500916.
- [125] J.-I. Kishine, A. S. Ovchinnikov, in *Solid State Physics*, (Eds: R. E. Camley, R. L. Stamps), Vol. 66, Academic Press, San Diego, United States **2015**, Ch. 1, pp. 1–130.
- [126] A. O. Leonov, C. Pappas, I. I. Smalyukh, *Phys. Rev. B* **2021**, *104*, 064432.
- [127] A. Chacon, L. Heinen, M. Halder, A. Bauer, W. Simeth, S. Mühlbauer, H. Berger, M. Garst, A. Rosch, C. Pfleiderer, *Nat. Phys.* **2018**, *14*, 936.
- [128] Y. Togawa, T. Koyama, K. Takayanagi, S. Mori, Y. Kousaka, J. Akimitsu, S. Nishihara, K. Inoue, A. S. Ovchinnikov, J. Kishine, *Phys. Rev. Lett.* **2012**, *108*, 107202.
- [129] S. Mühlbauer, B. Binz, F. Jonietz, C. Pfleiderer, A. Rosch, A. Neubauer, R. Georgii, P. Böni, *Science* **2009**, *323*, 915.
- [130] T. Schultz, R. Ritz, A. Bauer, M. Halder, M. Wagner, C. Franz, C. Pfleiderer, K. Everschor, M. Garst, A. Rosch, *Nat. Phys.* **2012**, *8*, 301.
- [131] E. A. Karhu, S. Kahwaji, M. D. Robertson, H. Fritzsche, B. J. Kirby, C. F. Majkrzak, T. L. Monchesky, *Phys. Rev. B* **2011**, *84*, 060404.
- [132] E. A. Karhu, U. K. Rößler, A. N. Bogdanov, S. Kahwaji, B. J. Kirby, H. Fritzsche, M. D. Robertson, C. F. Majkrzak, T. L. Monchesky, *Phys. Rev. B* **2012**, *85*, 094429.
- [133] M. N. Wilson, E. A. Karhu, D. P. Lake, A. S. Quigley, S. Meynell, A. N. Bogdanov, H. Fritzsche, U. K. Rößler, T. L. Monchesky, *Phys. Rev. B* **2013**, *88*, 214420.
- [134] B. Wiedemann, A. Chacon, S. L. Zhang, Y. Khaydukov, T. Hesjedal, O. Soltwedel, T. Keller, S. Mühlbauer, T. Adams, M. Halder, C. Pfleiderer, P. Böni, Reciprocal Space Mapping of Magnetic Order in Thick Epitaxial MnSi Films **2017**, <https://arxiv.org/abs/1710.00544> (accessed: October 2022).
- [135] N. Kanazawa, J. S. White, H. M. Rønnow, C. D. Dewhurst, Y. Fujishiro, A. Tsukazaki, Y. Kozuka, M. Kawasaki, M. Ichikawa, F. Kagawa, Y. Tokura, *Phys. Rev. B* **2016**, *94*, 184432.
- [136] N. A. Porter, C. S. Spencer, R. C. Temple, C. J. Kinane, T. R. Charlton, S. Langridge, C. H. Marrows, *Phys. Rev. B* **2015**, *92*, 144402.
- [137] N. A. Porter, P. Sinha, M. B. Ward, A. N. Dobrynin, R. M. D. Brydson, T. R. Charlton, C. J. Kinane, M. D. Robertson, S. Langridge, C. H. Marrows, **2013**, <https://arxiv.org/abs/1312.1722> (accessed: October 2022).
- [138] C. S. Spencer, J. Gayles, N. A. Porter, S. Sugimoto, Z. Aslam, C. J. Kinane, T. R. Charlton, F. Freimuth, S. Chadov, S. Langridge, J. Sinova, C. Felser, S. Blügel, Y. Mokrousov, C. H. Marrows, *Phys. Rev. B* **2018**, *97*, 214406.
- [139] S. A. Meynell, M. N. Wilson, K. L. Krycka, B. J. Kirby, H. Fritzsche, T. L. Monchesky, *Phys. Rev. B* **2017**, *96*, 054402.
- [140] T. Saerbeck, in *Solid State Physics*, (Eds: R. E. Camley, R. L. Stamps), Vol. 65, Academic Press, San Diego, United States **2014**, Ch. 3, pp. 237–352.
- [141] G. L. Causer, A. Chacon, A. Heinemann, C. Pfleiderer, *J. Appl. Crystallogr.* **2023**, *56*, <https://doi.org/10.1107/S1600576722010755>.
- [142] C. Moreau-Luchaire, C. Moutafis, N. Reyren, J. Sampaio, C. A. F. Vaz, N. V. Horne, K. Bouzehouane, K. Garcia, C. Deranlot, P. Warnicke, P. Wohlhüter, J.-M. George, M. Weigand, J. Raabe, V. Cros, A. Fert, *Nat. Nanotechnol.* **2016**, *11*, 444.
- [143] M. Hoffmann, J. Weischenberg, B. Dupé, F. Freimuth, P. Ferriani, Y. Mokrousov, S. Heinze, *Phys. Rev. B* **2015**, *92*, 020401.
- [144] O. Boule, J. Vogel, H. Yang, S. Pizzini, D. de Souza Chaves, A. Locatelli, T. O. Mendes, A. Sala, L. D. Buda-Prejbeanu, O. Klein, M. Belmeguenai, Y. Roussigne, A. Stashkevich, S. M. Cherif, L. Abelle, M. Foerster, M. Chshiev, S. Auffret, I. M. Miron, G. Gaudin, *Nat. Nanotechnol.* **2016**, *11*, 449.
- [145] D. A. Gilbert, B. B. Maranville, A. L. Balk, B. J. Kirby, P. Fischer, D. T. Pierce, J. Unguris, J. A. Borchers, K. Liu, *Nat. Commun.* **2015**, *6*, 8462.
- [146] J. Chen, W. Mao, L. Gao, F. Yan, T. Yajima, N. Chen, Z. Chen, H. Dong, B. Ge, P. Zhang, X. Cao, M. Wilde, Y. Jiang, T. Terai, J. Shi, *Adv. Mater.* **2020**, *32*, 1905060.
- [147] R. O. M. Aboljadayel, C. J. Kinane, C. A. F. Vaz, D. M. Love, R. S. Weatherup, P. Braeuninger-Weimer, M. B. Martin, A. Ionescu, A. J. Caruana, T. R. Charlton, J. Llandro, P. M. S. Monteiro, C. H. W. Barnes, S. Hofmann, S. Langridge, Determining the Proximity Effect Induced Magnetic Moment in Graphene by Polarized Neutron Reflectivity and X-ray Magnetic Circular Dichroism **2021**, <https://arxiv.org/abs/2101.09946> (accessed: October 2022).
- [148] M. Åberg, N. Ahlfors, R. Ainsworth, C. Alba-Simionesco, S. Alimov, N. Aliouane, B. Alling, K. G. Andersson, N. A. Andersen, B. R. Hansen, M. Jensen, E. B. Klinkby, E. Bergbäck Knudsen, B. Lauritzen, J. B. Nielsen, S. P. Nielsen, E. Nonbøl, P. Norby, H. F. Poulsen, S. O. Poulsen, O. Rasmussen, F. B. Saxild, G. Severin, P. K. Willendrup, *ESS Technical Design Report*, European Spallation Source, Lund, Sweden, **2013**.
- [149] A. Glavic, J. Stahn, S. Schütz, *Swiss Neutron News*, **2016** [https://sgn.web.psi.ch/sgn/snn/snn\\_48.pdf](https://sgn.web.psi.ch/sgn/snn/snn_48.pdf) (accessed October 2022).

[150] H. Shishido, A. Okumura, T. Saimyoji, S. Nakamura, S. Ohara, Y. Togawa, *Appl. Phys. Lett.* **2021**, 118, 102402.

[151] W. Kreuzpaintner, A. Schmehl, A. Book, T. Mairoser, J. Ye, B. Wiedemann, S. Mayr, J.-F. Moulin, J. Stahn, D. A. Gilbert,

H. Gabold, Z. Inanloo-Maranloo, M. Heigl, S. Masalovich, R. Georgii, M. Albrecht, J. Mannhart, P. Böni, *Phys. Status Solidi B* **2022**, 259, 2100153.



**Grace L. Causer** obtained her Ph.D. in physics from the University of Wollongong in 2018, and is currently a postdoc at the Technical University of Munich. Grace's scientific focus is the study of proximity effects in magnetic thin film heterostructures, as well as the study of topological skyrmions in bulk and epitaxial cubic chiral magnets. Her main research tools are polarized neutron reflectometry, small-angle neutron scattering, X-ray reflectometry and diffraction, as well as magnetometry and transport measurements.



**Laura Guasco** joined the Max Planck Institute for Solid State Research and obtained her Ph.D. in physics from the University of Stuttgart in 2022. Her research focuses on neutron and X-ray grazing incidence techniques, particularly polarized neutron reflectometry, for the study of hydrogen absorption and complex magnetism in thin film heterostructures.



**David Cortie** is a research scientist at the Australian Nuclear Science and Technology Organisation (ANSTO) specializing in the applications of polarized neutron reflectometry and neutron spectroscopy. His research focuses on the interplay between magnetism, electronic structure, and phonons in quantum materials including strongly correlated oxides, 2D materials, and topological semimetals. Prior to joining ANSTO, David was an Australian Research Council DECRA fellow and University of British Columbia-Max-Planck research fellow at the Stewart Blusson Quantum Matter Institute. He obtained his Ph.D. in physics from the University of Wollongong in 2013.